

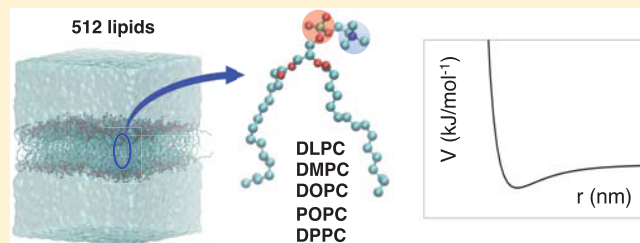
# Lipid Head Group Parameterization for GROMOS 54A8: A Consistent Approach with Protein Force Field Description

Irene Marzuoli,<sup>1</sup> Christian Margreitter,<sup>1</sup> and Franca Fraternali<sup>\*1,2</sup>

Randall Centre for Cell and Molecular Biology, King's College London, London SE1 1UL, U.K.

<sup>1</sup> Supporting Information

**ABSTRACT:** Membranes are a crucial component of both bacterial and mammalian cells, being involved in signaling, transport, and compartmentalization. This versatility requires a variety of lipid species to tailor the membrane's behavior as needed, increasing the complexity of the system. Molecular dynamics simulations have been successfully applied to study model membranes and their interactions with proteins, elucidating some crucial mechanisms at the atomistic detail and thus complementing experimental techniques. An accurate description of the functional interplay of the diverse membrane components crucially depends on the selected parameters that define the adopted force field. A coherent parameterization for lipids and proteins is therefore needed. In this work, we propose and validate new lipid head group parameters for the GROMOS 54A8 force field, making use of recently published parametrizations for key chemical moieties present in lipids. We make use additionally of a new canonical set of partial charges for lipids, chosen to be consistent with the parameterization of soluble molecules such as proteins. We test the derived parameters on five phosphocholine model bilayers, composed of lipid patches four times larger than the ones used in previous studies, and run 500 ns long simulations of each system. Reproduction of experimental data like area per lipid and deuterium order parameters is good and comparable with previous parameterizations, as well as the description of liquid crystal to gel-phase transition. On the other hand, the orientational behavior of the head groups is more realistic for this new parameter set, and this can be crucial in the description of interactions with other polar molecules. For that reason, we tested the interaction of the antimicrobial peptide lactoferricin with two model membranes showing that the new parameters lead to a weaker peptide–membrane binding and give a more realistic outcome in comparing binding to antimicrobial versus mammal membranes.



## 1. INTRODUCTION

Cellular membranes are key promoters and regulators of many biological processes due to their crucial role in segregating the external world from the organism. Small molecule transport, drug permeation, intracellular signaling, and antibody response are all regulated by the cell membrane or by membrane-related components.<sup>1–8</sup> To fully comprehend and ultimately influence the bespoke processes, it is paramount to understand membranes and their constituting lipids in atomistic detail. However, due to the complexity of those systems, researchers have resorted to the use of simplified model membranes, which can be synthesized and characterized *in vitro*. This enables the individual contributions of the components involved to be disentangled. Indeed, for the cellular membrane to be able to perform different functions, its composition is necessarily complex. Lipids are one of the main components and can be present in up to hundreds of different species.<sup>9</sup> In addition, many transmembrane proteins tessellate the cell surface, promoting signaling pathways and influencing the membrane's structural and mechanical properties.<sup>10,11</sup> Phospholipid bilayers and micelles have been investigated, in particular, as these lipids represent the main components of the eukaryotic and the inner bacterial membranes. Both have been modeled selecting

specific phospholipids to emulate the appropriate surface charge or to reproduce the human cell membrane fluidity by introducing, for example, cholesterol.<sup>12,13</sup> As these simplified membranes retain the core characteristics of their different biological templates,<sup>14</sup> they can be used to test the membrane interaction with proteins, peptides, antimicrobial molecules, or drugs.

Experiments can provide global properties of membranes and, despite the great accuracy of techniques like NMR and X-ray scattering in measuring the average position of atoms in rigid structures, they face challenges when characterizing the biologically relevant fluid phase, as opposed to the gel one that emerges at lower temperatures.<sup>15–18</sup> Alongside experimental characterization, molecular dynamic (MD) simulations have played a central role in the investigation of the behavior of lipids, due to the atomistic spatial resolution they provide. Therefore, MD simulations complement our understanding of membranes' behavior and are also important for the study of lipid systems in combination with proteins, providing detailed insights into the mechanisms of their interactions. In the past,

Received: May 25, 2019

Published: August 21, 2019

70 MD simulations have been successfully employed to reproduce  
 71 typical phenomena in membranes, such as lipids' flip-flop,<sup>19,20</sup>  
 72 vesicle formation,<sup>21,22</sup> aggregation into bilayers,<sup>23–25</sup> and  
 73 stress-induced<sup>26–29</sup> and peptide-induced pore formations.<sup>30–32</sup>  
 74 Moreover, the implementation of more realistic models of  
 75 bacterial membranes, by including a more diverse set of  
 76 components into the simulated systems, has been pursued<sup>33,34</sup>  
 77 to test specific interactions with antimicrobial peptides and  
 78 understand their selectivity.<sup>35,36</sup>

79 The reliability of such simulations depends on the accurate  
 80 parameterizations of lipids and proteins, which need to be  
 81 validated against experimental data. Moreover, the two  
 82 descriptions must be consistently integrated into the force  
 83 fields used, i.e., be derived with the same parameterization  
 84 procedure. Different approaches to the problem are possible,  
 85 which resulted in the development of multiple force fields  
 86 suitable for simulations of biomolecules: for example, the  
 87 CHARMM<sup>37–39</sup> and AMBER<sup>40</sup> force fields are parameterized  
 88 from quantum mechanics calculations, while GROMOS96<sup>41</sup> is  
 89 calibrated to match global properties like the hydration free  
 90 energy of chemical moieties. All of them have been constantly  
 91 updated to meet the new experimental values available and  
 92 more faithfully reproduce the different species involved.

93 However, it is a very difficult task to parameterize the  
 94 constituents of a complex system so that all parameters are  
 95 consistent with the rest of the force field and reproduce both  
 96 the single-molecule observables and the collective behavior. In  
 97 the present work, we consider the parameterization of  
 98 phospholipids in the context of the GROMOS96 force  
 99 field,<sup>41</sup> addressing some of the inconsistencies in the lipid  
 100 head group parameters commonly used so far, particularly in  
 101 consideration that these contribute to the description of  
 102 recognition processes at the interface.

103 In the past, lipid simulations using the GROMOS96 force  
 104 field suffered from difficulties involved in transferring the pre-  
 105 existing parameters, calibrated mainly for peptides in an  
 106 aqueous environment, to the amphiphilic environment of the  
 107 lipid assembly. This resulted in the failure to reproduce the  
 108 membranes' behavior properly<sup>42–44</sup> and therefore a series of  
 109 modifications were adopted, particularly in the choice of lipid-  
 110 specific Lennard-Jones interactions<sup>44–46</sup> and partial charges.<sup>42</sup>

111 In the light of recent reparameterizations of a set of choline  
 112 moieties<sup>47</sup> and of phosphate-containing species,<sup>48</sup> we under-  
 113 take the task of updating the parameters used for lipids, in  
 114 particular, phosphocholines, as they contain both these  
 115 chemical moieties. Within this work, we show that it is  
 116 possible to integrate the recently computed partial charges  
 117 within simulations while maintaining good agreement with the  
 118 available experimental data. We also test the transferability of  
 119 the new phosphate charges onto lipids without a choline head  
 120 group, namely, phosphoethanolamine (POPE) and phospha-  
 121 tidylglycerol (POPG).

122 Most importantly, the new description of phosphocholine is  
 123 consistent with the GROMOS96 parameterization philosophy,  
 124 based on the decomposition of large molecules into smaller  
 125 compounds and subsequently fitting their parameters to  
 126 experimental hydration free energies. Together with adjust-  
 127 ments to specific van der Waals potentials, we believe that the  
 128 parameters presented here will contribute to improving the  
 129 accuracy of the description of membrane–solvent and  
 130 membrane–protein interactions. To this aim, we compared  
 131 the available parameters with the one proposed in this work,  
 132 simulating the interaction of an antimicrobial peptide with two

model membranes, highlighting the differences in the  
 133 mechanisms observed, and comparing them with the available  
 134 experimental evidence.  
 135

## 2. METHODS

2.1. Background to Lipid Force Fields. The most recent iteration of the lipids' parameters commonly used in simulations with the GROMOS force field is the one by Poger and Mark.<sup>44</sup> They employed partial charges derived quantum-mechanically by Chiu et al.,<sup>42</sup> combined with a modified repulsion between the choline methyl groups and the OM oxygen atoms in the phosphate with respect to the standard choline–OM one.  
 143

The original set of Chiu charges<sup>42</sup> was derived from ab initio Hartree–Fock self-consistent field calculations<sup>52</sup> and Mulliken population analysis.<sup>53</sup> Slight modifications were applied to make each individual charge group sum up to an integer value, following the GROMOS96 philosophy. Despite the resulting charges that differ substantially from the ones used for the same chemical groups in different chemical contexts, the GROMOS community employed this set as it gave results in closer agreement with the available experimental data.  
 144 145 146 147 148 149 150 151 152 153 154 155 156 157 158 159 160 161 162 163 164 165 166 167 168 169 170 171 172 173 174 175 176 177 178 179 180 181 182 183 184 185 186 187 188 189 190 191 192 193 194 195 196 197 198 199 200 201 202 203 204 205 206 207 208 209 210 211 212 213 214 215 216 217 218 219 220 221 222 223 224 225 226 227 228 229 230 231 232 233 234 235 236 237 238 239 240 241 242 243 244 245 246 247 248 249 250 251 252 253 254 255 256 257 258 259 260 261 262 263 264 265 266 267 268 269 270 271 272 273 274 275 276 277 278 279 280 281 282 283 284 285 286 287 288 289 290 291 292 293 294 295 296 297 298 299 300 301 302 303 304 305 306 307 308 309 310 311 312 313 314 315 316 317 318 319 320 321 322 323 324 325 326 327 328 329 330 331 332 333 334 335 336 337 338 339 340 341 342 343 344 345 346 347 348 349 350 351 352 353 354 355 356 357 358 359 360 361 362 363 364 365 366 367 368 369 370 371 372 373 374 375 376 377 378 379 380 381 382 383 384 385 386 387 388 389 390 391 392 393 394 395 396 397 398 399 400 401 402 403 404 405 406 407 408 409 410 411 412 413 414 415 416 417 418 419 420 421 422 423 424 425 426 427 428 429 430 431 432 433 434 435 436 437 438 439 440 441 442 443 444 445 446 447 448 449 450 451 452 453 454 455 456 457 458 459 460 461 462 463 464 465 466 467 468 469 470 471 472 473 474 475 476 477 478 479 480 481 482 483 484 485 486 487 488 489 490 491 492 493 494 495 496 497 498 499 500 501 502 503 504 505 506 507 508 509 510 511 512 513 514 515 516 517 518 519 520 521 522 523 524 525 526 527 528 529 530 531 532 533 534 535 536 537 538 539 540 541 542 543 544 545 546 547 548 549 550 551 552 553 554 555 556 557 558 559 560 561 562 563 564 565 566 567 568 569 570 571 572 573 574 575 576 577 578 579 580 581 582 583 584 585 586 587 588 589 5810 5811 5812 5813 5814 5815 5816 5817 5818 5819 5820 5821 5822 5823 5824 5825 5826 5827 5828 5829 5830 5831 5832 5833 5834 5835 5836 5837 5838 5839 5840 5841 5842 5843 5844 5845 5846 5847 5848 5849 5850 5851 5852 5853 5854 5855 5856 5857 5858 5859 5860 5861 5862 5863 5864 5865 5866 5867 5868 5869 5870 5871 5872 5873 5874 5875 5876 5877 5878 5879 5880 5881 5882 5883 5884 5885 5886 5887 5888 5889 5890 5891 5892 5893 5894 5895 5896 5897 5898 5899 58100 58101 58102 58103 58104 58105 58106 58107 58108 58109 58110 58111 58112 58113 58114 58115 58116 58117 58118 58119 58120 58121 58122 58123 58124 58125 58126 58127 58128 58129 58130 58131 58132 58133 58134 58135 58136 58137 58138 58139 58140 58141 58142 58143 58144 58145 58146 58147 58148 58149 58150 58151 58152 58153 58154 58155 58156 58157 58158 58159 58160 58161 58162 58163 58164 58165 58166 58167 58168 58169 58170 58171 58172 58173 58174 58175 58176 58177 58178 58179 58180 58181 58182 58183 58184 58185 58186 58187 58188 58189 58190 58191 58192 58193 58194 58195 58196 58197 58198 58199 581910 581911 581912 581913 581914 581915 581916 581917 581918 581919 581920 581921 581922 581923 581924 581925 581926 581927 581928 581929 581930 581931 581932 581933 581934 581935 581936 581937 581938 581939 581940 581941 581942 581943 581944 581945 581946 581947 581948 581949 581950 581951 581952 581953 581954 581955 581956 581957 581958 581959 581960 581961 581962 581963 581964 581965 581966 581967 581968 581969 581970 581971 581972 581973 581974 581975 581976 581977 581978 581979 581980 581981 581982 581983 581984 581985 581986 581987 581988 581989 581990 581991 581992 581993 581994 581995 581996 581997 581998 581999 5819100 5819101 5819102 5819103 5819104 5819105 5819106 5819107 5819108 5819109 5819110 5819111 5819112 5819113 5819114 5819115 5819116 5819117 5819118 5819119 58191100 58191101 58191102 58191103 58191104 58191105 58191106 58191107 58191108 58191109 58191110 58191111 58191112 58191113 58191114 58191115 58191116 58191117 58191118 58191119 581911100 581911101 581911102 581911103 581911104 581911105 581911106 581911107 581911108 581911109 581911110 581911111 581911112 581911113 581911114 581911115 581911116 581911117 581911118 581911119 5819111100 5819111101 5819111102 5819111103 5819111104 5819111105 5819111106 5819111107 5819111108 5819111109 5819111110 5819111111 5819111112 5819111113 5819111114 5819111115 5819111116 5819111117 5819111118 5819111119 58191111100 58191111101 58191111102 58191111103 58191111104 58191111105 58191111106 58191111107 58191111108 58191111109 58191111110 58191111111 58191111112 58191111113 58191111114 58191111115 58191111116 58191111117 58191111118 58191111119 581911111100 581911111101 581911111102 581911111103 581911111104 581911111105 581911111106 581911111107 581911111108 581911111109 581911111110 581911111111 581911111112 581911111113 581911111114 581911111115 581911111116 581911111117 581911111118 581911111119 5819111111100 5819111111101 5819111111102 5819111111103 5819111111104 5819111111105 5819111111106 5819111111107 5819111111108 5819111111109 5819111111110 5819111111111 5819111111112 5819111111113 5819111111114 5819111111115 5819111111116 5819111111117 5819111111118 5819111111119 58191111111100 58191111111101 58191111111102 58191111111103 58191111111104 58191111111105 58191111111106 58191111111107 58191111111108 58191111111109 58191111111110 58191111111111 58191111111112 58191111111113 58191111111114 58191111111115 58191111111116 58191111111117 58191111111118 58191111111119 581911111111100 581911111111101 581911111111102 581911111111103 581911111111104 581911111111105 581911111111106 581911111111107 581911111111108 581911111111109 581911111111110 581911111111111 581911111111112 581911111111113 581911111111114 581911111111115 581911111111116 581911111111117 581911111111118 581911111111119 5819111111111100 5819111111111101 5819111111111102 5819111111111103 5819111111111104 5819111111111105 5819111111111106 5819111111111107 5819111111111108 5819111111111109 5819111111111110 5819111111111111 5819111111111112 5819111111111113 5819111111111114 5819111111111115 5819111111111116 5819111111111117 5819111111111118 5819111111111119 58191111111111100 58191111111111101 58191111111111102 58191111111111103 58191111111111104 58191111111111105 58191111111111106 58191111111111107 58191111111111108 58191111111111109 58191111111111110 58191111111111111 58191111111111112 58191111111111113 58191111111111114 58191111111111115 58191111111111116 58191111111111117 58191111111111118 58191111111111119 581911111111111100 581911111111111101 581911111111111102 581911111111111103 581911111111111104 581911111111111105 581911111111111106 581911111111111107 581911111111111108 581911111111111109 581911111111111110 581911111111111111 581911111111111112 581911111111111113 581911111111111114 581911111111111115 581911111111111116 581911111111111117 581911111111111118 581911111111111119 5819111111111111100 5819111111111111101 5819111111111111102 5819111111111111103 5819111111111111104 5819111111111111105 5819111111111111106 5819111111111111107 5819111111111111108 5819111111111111109 5819111111111111110 5819111111111111111 5819111111111111112 5819111111111111113 5819111111111111114 5819111111111111115 5819111111111111116 5819111111111111117 5819111111111111118 5819111111111111119 58191111111111111100 58191111111111111101 58191111111111111102 58191111111111111103 58191111111111111104 58191111111111111105 58191111111111111106 58191111111111111107 58191111111111111108 58191111111111111109 58191111111111111110 58191111111111111111 58191111111111111112 58191111111111111113 58191111111111111114 58191111111111111115 58191111111111111116 58191111111111111117 58191111111111111118 58191111111111111119 581911111111111111100 581911111111111111101 581911111111111111102 581911111111111111103 581911111111111111104 581911111111111111105 581911111111111111106 581911111111111111107 581911111111111111108 581911111111111111109 581911111111111111110 581911111111111111111 581911111111111111112 581911111111111111113 581911111111111111114 581911111111111111115 581911111111111111116 581911111111111111117 581911111111111111118 581911111111111111119 5819111111111111111100 5819111111111111111101 5819111111111111111102 5819111111111111111103 5819111111111111111104 5819111111111111111105 5819111111111111111106 5819111111111111111107 5819111111111111111108 5819111111111111111109 5819111111111111111110 5819111111111111111111 5819111111111111111112 5819111111111111111113 5819111111111111111114 5819111111111111111115 5819111111111111111116 5819111111111111111117 5819111111111111111118 5819111111111111111119 58191111111111111111100 58191111111111111111101 58191111111111111111102 58191111111111111111103 58191111111111111111104 58191111111111111111105 58191111111111111111106 58191111111111111111107 58191111111111111111108 58191111111111111111109 58191111111111111111110 58191111111111111111111 58191111111111111111112 58191111111111111111113 58191111111111111111114 58191111111111111111115 58191111111111111111116 58191111111111111111117 58191111111111111111118 58191111111111111111119 581911111111111111111100 581911111111111111111101 581911111111111111111102 581911111111111111111103 581911111111111111111104 581911111111111111111105 581911111111111111111106 581911111111111111111107 581911111111111111111108 581911111111111111111109 581911111111111111111110 581911111111111111111111 581911111111111111111112 581911111111111111111113 581911111111111111111114 581911111111111111111115 581911111111111111111116 581911111111111111111117 581911111111111111111118 581911111111111111111119 5819111111111111111111100 5819111111111111111111101 58191111111

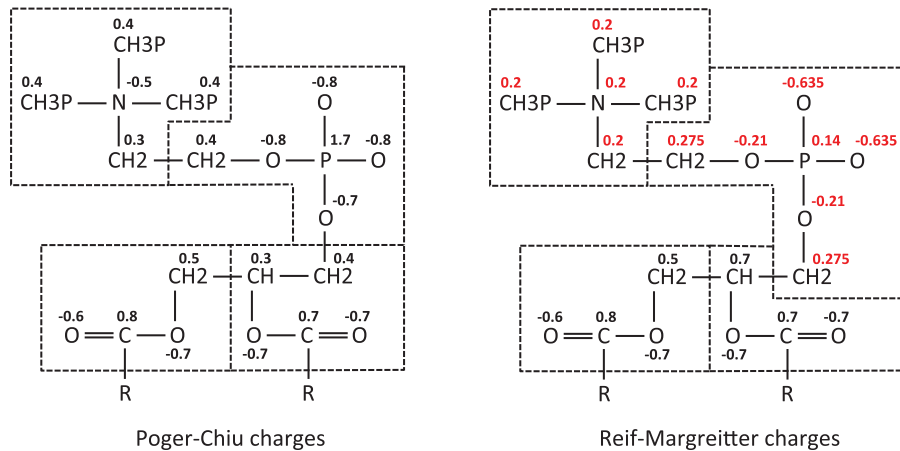


**Figure 2.** Partial charges for the phosphocholine head groups and the glycerol and ester moieties in the Chiu<sup>42</sup> scheme (left) and the one tested in the current work (right). Red font denotes values that have been changed between the two. Atoms belonging to the same charge groups are enclosed by the same dashed polygon.

**Table 1. Table of Simulations for Phosphocholine Bilayers<sup>a</sup>**

sim	charges <sup>b</sup>	FF	simulations of phosphocholine lipids	
			CH3p–OM C12 <sup>c</sup> (kJ mol <sup>-1</sup> nm <sup>12</sup> )	CH3p–CH3p C12 <sup>d</sup> (kJ mol <sup>-1</sup> nm <sup>12</sup> )
1	Chiu	S4A7	$1.58 \times 10^{-5}$	$2.66 \times 10^{-5}$
2	Chiu	S4A8	$6.93 \times 10^{-6}$	$6.48 \times 10^{-5}$
3	RM	S4A8_v1	$1.10 \times 10^{-5}$	$6.48 \times 10^{-5}$
4	RM	S4A8_v2	$1.58 \times 10^{-5}$	$6.48 \times 10^{-5}$
5	RM	S4A8_v3	$4.50 \times 10^{-5}$	$6.48 \times 10^{-5}$

<sup>a</sup>All are run for 500 ns and systems consisting of 500 lipid molecules (256 per layer), using a particle mesh Ewald (PME) long-range electrostatic scheme. <sup>b</sup>Charge set: Chiu from Ref 42, Reif–Margreitter (RM) as illustrated in the present work. <sup>c</sup>As a reference, the standard C12 parameter in S4A7/S4A8 for CH3–OM is  $4.44 \times 10^{-6}$  kJ mol<sup>-1</sup> nm<sup>12</sup>. <sup>d</sup>The CH3–CH3 C12 parameters are  $2.66 \times 10^{-5}$  for each parameter set.

the united methyl atoms in the choline head group of lipids<sup>167</sup> and the oxygen-type OM, present in the phosphate group, was<sup>168</sup> increased by a factor of 3.5. This modification was optimized<sup>169</sup> and tested against experimental values, increases the spacing<sup>170</sup> between individual lipids, and thus leads to the appropriate<sup>171</sup> area per lipid (ApL).<sup>51,54</sup> The new atom-type CH3p has all of<sup>172</sup> the characteristics of CH3, except for the bespoke parameter,<sup>173</sup> i.e., all Lennard-Jones interactions involving OM. These<sup>174</sup> Poger–Chiu parameters have been successful in reproducing<sup>175</sup> membrane behavior and were used in many MD applica-<sup>176</sup>  
tions.<sup>33,55</sup>

Later, Reif et al.<sup>47</sup> enhanced the methyl–methyl repulsion<sup>178</sup> for both CH3 and CH3p in the S4A8 parameter set, which<sup>179</sup> allowed for a decrease in the large repulsion value between<sup>180</sup> CH3p and OM previously introduced<sup>44</sup> while still reproducing<sup>181</sup> experimental values. The S4A8 parameter set contains two<sup>182</sup> additional, nonlipid-specific, modifications important for this<sup>183</sup> work: the choline Lennard-Jones parameters and partial<sup>184</sup> charges, and the phosphate partial charges. The C12<sup>185</sup> Lennard-Jones repulsion term for the NL nitrogen atom type<sup>186</sup> (present in the choline moiety) was increased to successfully<sup>187</sup> prevent oversolvation.<sup>47,54</sup> To the same end, the +1 e total<sup>188</sup> charge was evenly distributed over all five atoms, which<sup>189</sup> resulted in a better approximation of the experimentally<sup>190</sup> obtained hydration free energy in comparison to the S4A7<sup>191</sup> parameter set. Similarly, Margreitter et al.<sup>48</sup> calibrated the<sup>192</sup> partial charges of four phosphate species and enhanced the<sup>193</sup> reproduction of experimental data. The relevant phosphate-<sup>194</sup> containing species for this work is dimethyl-phosphate, a<sup>195</sup>

compound not directly present in force field versions prior to 196 S4A8.<sup>197</sup>

Another approach to lipid parameterization was proposed by 198 Kukol,<sup>46</sup> namely, the use of the already available CH0 atom 199 type for the ester carbons in place of the standard C atom type,<sup>200</sup> in conjunction with the Chiu charges. This atom type,<sup>201</sup> designed to describe a bare sp<sup>3</sup> carbon bound to four heavy<sup>202</sup> atoms, has a repulsion energy term 10–40 times larger than a<sup>203</sup> bare carbon bound to other atom types, enforcing a greater<sup>204</sup> spacing between lipid molecules and thereby increasing the<sup>205</sup> ApL. As this modification is also applicable in the absence of a<sup>206</sup> choline head group and does not require the introduction of<sup>207</sup> another atom type, this method can be used to parameterize<sup>208</sup> POPE and POPG.<sup>209</sup>

**2.2. Parameterization Strategy.** In an effort to enhance<sup>210</sup> the consistency of the force field, we integrated the new partial<sup>211</sup> charges for the choline and phosphate moieties [Reif–<sup>212</sup> Margreitter (RM) charge set] into the lipid building blocks<sup>213</sup> of GROMOS 54A8 so that the entire phosphocholine head<sup>214</sup> group now follows the common GROMOS-like modeling<sup>215</sup> approach (Figure 2). Only the partial charges of the ester<sup>216</sup> groups remain as described in the Chiu set, a deviation from<sup>217</sup> the canonical parameterization strategy necessary to match the<sup>218</sup> experimental area per lipid values: Chandrasekhar et al.<sup>219</sup> showed in ref 56 that the replacement of the ester charges<sup>220</sup> with the standard ones for the ester moiety (parameterized to<sup>221</sup> reproduce the experimental free energies of hydration of a<sup>222</sup> series of alkane esters<sup>57</sup>) resulted in a much smaller area per<sup>223</sup> lipid, not compatible with the experimental values.<sup>224</sup>

The introduction of the new head group charges required a refinement of the CH<sub>3</sub>p–OM Lennard-Jones repulsion, as the S4A8 value was set considering the original Chiu charges. Ideally, one would always try to keep the force field terms as much transferable as possible. Nevertheless, the complexity and anisotropic nature of some biological environments can be difficult to parametrize with single chemical groups, as the same chemical group can behave differently according to the context it is inserted in. Lipid systems are one of such examples, and to maintain the correct physical behavior of the system, we used specific C12 parameters for the CH<sub>3</sub>p–OM repulsion in phosphocholine lipid atoms. This allows for a more balanced description of the physicochemical properties of the lipid bilayer and a better match with the available experimental observables.

Aiming at this, and to disentangle the effect of charge parameterization versus the CH<sub>3</sub>p–OM repulsion, we tested three different values of such Lennard-Jones parameter with the new charges while control simulations were run using the Chiu partial charges and the GROMOS S4A7 or S4A8 parameter set for each lipid (Table 1). The phosphocholines tested are 1,2-lauroyl-*sn*-glycero-3-phosphocholine (DLPC), 1,2-dimyristoyl-*sn*-glycero-3-phosphocholine (DMPC), 1,2-dioleoyl-*sn*-glycero-3-phosphocholine (DOPC), 1,2-dipalmitoyl-*sn*-glycero-3-phosphocholine (DPPC), and 2-oleoyl-1-palmitoyl-*sn*-glycero-3-phosphocholine (POPC), which have different tail lengths and numbers of unsaturated bonds as in previous works<sup>44,58</sup> (Table 2).

**Table 2. Details of the Systems Simulated: Lipid Name, Tail Composition, Initial ApL (and Reference from Which the Initial Coordinates Are Taken), Simulation Temperature, and Gel–Liquid Phase Experimental Transition Temperature**

lipid bilayer systems				
lipid <sup>a</sup>	tails <sup>b</sup>	ApL <sub>0</sub> (nm <sup>2</sup> )	T <sub>MD</sub> (K)	T <sub>C</sub> (K)
DLPC	12:0/12:0	0.632 <sup>44</sup>	303	276.4 <sup>63–66</sup>
DMPC	14:0/14:0	0.616 <sup>58</sup>	303	296.9 <sup>63–66</sup>
DOPC	18:1c9/18:1c9	0.649 <sup>58</sup>	303	255.7 <sup>63–66</sup>
POPC	16:0/18:1c9	0.638 <sup>58</sup>	303	270.5 <sup>63–66</sup>
DPPC	16:0/16:0	0.631 <sup>58</sup>	323	314.2 <sup>63–66</sup>
POPE	16:0/18:1c9	0.568 <sup>33</sup>	313	299.3 <sup>67</sup>
POPG	16:0/18:1c9	0.602 <sup>33</sup>	303	268.1 <sup>68</sup>

<sup>a</sup>DLPC: 1,2-lauroyl-*sn*-glycero-3-phosphocholine, DMPC: 1,2-dimyristoyl-*sn*-glycero-3-phosphocholine, DOPC: 1,2-dioleoyl-*sn*-glycero-3-phosphocholine, POPC: 2-oleoyl-1-palmitoyl-*sn*-glycero-3-phosphocholine, DPPC: 1,2-dipalmitoyl-*sn*-glycero-3-phosphocholine, POPE: 1-palmitoyl-2-oleoyl-*sn*-glycero-3-phosphoethanolamine, POPG: 1-palmitoyl-2-oleoyl-*sn*-glycero-3-phospho-(1'-rac-glycerol). <sup>b</sup>Example: 16:0/18:1c9 indicates that tail 1 has 16 carbons with no unsaturated bonds and tail 2 has 18 carbons with one unsaturated bond between carbons 9 and 10—ester carbon counts as number 1.

To prove the transferability of the new phosphate charges to other lipid species, which do not contain a choline head group (and thus an enhanced repulsion, which has an impact on the ApL), test simulations of a phosphoethanolamine (POPE) and a phosphoglycerol (POPG, Table 2) bilayer have been performed. These lipids have amine and glycerol head groups, respectively. The parameterization of both takes advantage of the Kukol approach<sup>46</sup> employing a CH<sub>0</sub> atom for the ester moieties to enhance the repulsion between lipids. For POPE

and POPG, simulations were run with the standard parameters from ref 33 (denoted as Piggot–Chiu in the present work) or with the updated phosphate partial charges (Supporting Information (SI) Table 2).

The evolution of simulation techniques seen in the recent years suggested two other changes in the simulation setup: first, the original set of parameters was designed to be used with a twin-range cutoff scheme and a reaction field long-range electrostatic contribution,<sup>59</sup> but the twin-range cutoff is no longer supported in the latest versions of the GROMACS software used for the present work.<sup>60</sup> Additionally, the PME algorithm<sup>61</sup> for long-range electrostatic treatment is currently the predominant method used for protein dynamics. In the context of unifying the two fields of protein and lipid simulations, we therefore opted for a PME long-range treatment, running a control simulation (on the DPPC bilayer) with a reaction field scheme to assess the impact of such a change (SI Table 1).

The other change we adopted in comparison to the earlier work was a larger system size. Due to computational limitations, the original parameterization was performed on a 128-lipid bilayer,<sup>44</sup> but recent advances allow for larger systems to be simulated and we therefore used membranes four times as large (512 lipids). This larger size allows to track larger undulations of the membrane, as the effect of periodic boundary conditions (PBCs) is less restrictive. Again, a control simulation on a 128 DPPC membrane has been run to test the relevance and the effect of this change (SI Table 1).

Finally, the improvements reached with the adoption of the new parameters are monitored through the comparison with experimental values, but it is useful to have benchmarks derived from other simulation experiments. For that purpose, we compare some key properties with the values obtained by the all-atom CHARMM36 force field.<sup>37,62</sup> Despite a thorough comparison beyond the present work, it is relevant to observe whether the changes introduced by the new parameters are going in the direction of the outcomes proposed by other descriptions.

**2.3. Simulation Systems.** Seven pure lipid bilayers have been simulated, five of which contain phosphocholines, one phosphoethanolamine (POPE), and one phosphoglycerol (POPG), as described in Table 2. Every bilayer is formed by 512 lipids (256 per leaflet), generated by replicating an equilibrated 128-lipid system from the literature two times in the *x* and *y* directions (see Table 2).

Water molecules were added to reach a minimum distance of 7.5 nm between periodic copies of the membrane along the *z*-direction, with a ratio of 85–120 H<sub>2</sub>O per lipid. This distance is larger than the one used in the previous parameterization publications because we observed an enhanced undulatory behavior for larger membranes and therefore a higher distance is necessary to avoid interactions between periodic replicas in the *z*-direction.

**2.4. Simulation Parameters.** All simulations were run using the GROMACS software version 2016.3,<sup>60,69,70</sup> under periodic boundary conditions in a rectangular box. The temperature was maintained by coupling the membrane and the solvent independently to an external bath using the Berendsen thermostat<sup>71</sup> with a coupling time  $\tau_T$  of 0.1 ps, at the reference temperatures indicated in Table 2, which are above the gel–liquid phase transition temperature for each lipid. The pressure was kept at 1 bar with a semi-isotropic coupling using a Berendsen barostat,<sup>71</sup> applying isothermal coupling

325 compressibility of  $4.5 \times 10^{-5}$  bar $^{-1}$  and a coupling constant  $\tau_p$   
 326 of 0.5 ps. Covalent bond lengths of the lipids were constrained  
 327 using the LINCS algorithm.<sup>72</sup> The geometry of the simple  
 328 point charge water molecules was constrained using  
 329 SETTLE.<sup>73</sup> A 2 fs time step was used, with a Verlet integration  
 330 scheme. The PME<sup>61</sup> long-range treatment was applied to the  
 331 electrostatic interactions beyond a 1.4 nm cutoff, and the  
 332 reaction field scheme<sup>59</sup> control simulation was run with the  
 333 same cutoff radius. A plain cutoff was used for van der Waals  
 334 interactions, with a cutoff radius of 1.4 nm.

335 Each system was initially energy-minimized and then  
 336 simulated at 50 K for 10 ps. Subsequently, the temperature  
 337 was increased gradually over 500 ps until the final simulation  
 338 temperature. The system was then simulated for 500 ns. The  
 339 equilibration of the systems was monitored by examining the  
 340 time evolution of the potential energy and the area per lipid:  
 341 200 ns is found to be sufficient to reach equilibration for all of  
 342 the bilayers (SI Figure 2) so that the analysis has been  
 343 performed over the last 300 ns of the production run, with  
 344 frames stored every 100 ps. An overview of the simulations  
 345 performed is given in Table 1 and SI Tables 1 and 2.

346 **2.5. Analysis.** To calibrate the lipid parameters, we used  
 347 the observables listed below, as common practice in standard  
 348 parameterization procedures.<sup>58,74</sup>

349 **2.5.1. Area per Lipid.** For systems where the membrane is  
 350 aligned to the  $xy$  plane, the area per lipid (ApL) can be  
 351 computed from the product of the lateral dimensions of the  
 352 simulation box divided by the number of lipids in one leaflet.  
 353 As shown in SI Figure 2 for DPPC, after 100 ns of simulation,  
 354 the ApL oscillates around a value with fluctuations of the same  
 355 magnitude, indicating equilibration. To allow further time for  
 356 local rearrangements, we restrict our analyses to the last 300 ns  
 357 of the simulations.

358 The equilibration protocol was verified on the DPPC  
 359 bilayer, repeating the computation of the ApL on two  
 360 nonoverlapping time windows, specifically between 200 and  
 361 350 ns and between 350 and 500 ns. For all of the parameter  
 362 sets, the two windows gave compatible values of the ApL,  
 363 confirming the convergence of the simulations (SI Figure 3).  
 364 The above procedure is valid if the membrane is flat or has  
 365 minor undulations only. To test this and verify that deviations  
 366 from planarity are not influencing the results, the ApL was  
 367 recomputed taking into account membrane undulations  
 368 according to the procedure outlined in ref 75. The differences  
 369 with the values computed from the simulation box dimensions  
 370 were between 0.20 and 0.46%, which is lower than the error  
 371 derived from the standard deviation across the simulation for  
 372 any of the area per lipid computed.

373 As such, our computations are of value in rating the results  
 374 against experimental outcomes and/or to compare parameter  
 375 sets, as a local measure would not significantly improve the  
 376 comparison.

377 **2.5.2. Isothermal Area Compressibility Module.** Following  
 378 the protocol in ref 58, we computed the isothermal area  
 379 compressibility module ( $K_A$ ) from the fluctuations of the ApL  
 380 values according to

$$K_A = \frac{k_B \langle T \rangle \langle \text{ApL} \rangle}{n_L \sigma_{\text{ApL}}^2} \quad (1)$$

382 where  $k_B$  is the Boltzmann constant,  $\langle T \rangle$  and  $\langle \text{ApL} \rangle$  are the  
 383 ensemble averages of the temperature and the area per lipid,

respectively,  $n_L$  is the number of lipids in one leaflet, and  $\sigma_{\text{ApL}}^2$  is the variance of ApL.

386 **2.5.3. Bilayer Thickness.** From the electron density profiles,  
 387 the bilayer thickness can be evaluated in several ways and  
 388 compared to the values from X-ray scattering experiments: the  
 389 hydrophobic thickness ( $D_{\text{HH}}$ ) is measured as the distance  
 390 between the phosphorus peaks in the two layers, as these  
 391 atoms have the highest electron density, while the Luzzati  
 392 thickness ( $D_B$ )<sup>58</sup> is defined as

$$D_B = b_z - \int_{-b_z/2}^{+b_z/2} \rho_W(z) dz \quad (2)$$

394 where  $b_z$  is the  $z$ -dimension of the simulation box and  $\rho_W(z)$  is  
 395 the volume fraction of water (vs other components) along  $z$   
 396 and normalized to 1 in the bulk water region

$$\rho_W(z) = \frac{n_W(z)V_W}{dV} \quad (3)$$

398 where  $n_W(z)$  is the time-averaged number of water molecules  
 399 in a bin of width  $dz$ ,  $V_W$  is the specific volume of the water  
 400 model used (taken from ref 76), and  $dV$  is the time-averaged  
 401 volume of a slice.

402 **2.5.4. Dipole Potential.** The dipole potential along the  $z$ -  
 403 direction (perpendicular to the membrane plane) can be  
 404 computed from the charge density along  $z$  ( $\rho(z)$ ) via a double  
 405 integration<sup>77</sup>

$$\psi(z) = -\frac{1}{\epsilon_0} \int_{z_0}^z \int z_0^z \rho(z'') dz'' dz' \quad (4)$$

507 Several choices are possible for the two integration constants,<sup>78</sup>  
 508 and for the present work, they are selected to set the dipole  
 509 potential to zero in the middle of the bulk water region, at both  
 510 sides of the membrane.

511 **2.5.5. Deuterium Order Parameter of Lipid Chains.** The  
 512 deuterium order parameters  $S_{CD}$  of the acyl chains for each  
 513 lipid bilayer were calculated and compared between the  
 514 different sets studied.  $S_{CD}$  evaluates the average order of the  
 515 lipid tails by measuring the orientation with respect to the  
 516 bilayer normal of a carbon–hydrogen bond in a given position  
 517 along the chain for each lipid in the bilayer. Their spread is  
 518 evaluated according to the ensemble average

$$S_{CD} = \frac{1}{2} \langle 3 \cos^2 \theta - 1 \rangle \quad (5)$$

707 As the GROMOS force field employs a united-atom  
 708 representation, the tetrahedral positions of the hydrogens are  
 709 constructed based on the neighboring carbons' positions.

710 **2.5.6. Hydration of Head Groups.** To estimate and  
 711 compare the hydration of lipid molecules, we computed the  
 712 distribution of the distances between the oxygen of water and  
 713 the nearest lipid atom. For each individual chemical group, the  
 714 distance between the water oxygen and the nearest atom  
 715 within that group was calculated. A quantitative measure for  
 716 hydration was obtained by integrating the distribution up to  
 717 the first peak or second one (for phosphate and glycerol).

718 **2.5.7. Orientation of Head Groups.** We computed the  
 719 orientation of the lipids' head groups as the distribution of the  
 720 angle between the P–N vector (joining the phosphorus atom  
 721 and the choline nitrogen) and the outward normal to the  
 722 membrane. The orientation of the *sn*-1 and -2 carbonyl dipoles  
 723 with respect to the bilayer normal has also been calculated.

**Table 3.** Average Area per Lipid (in nm<sup>2</sup>) over the Last 300 ns of Simulations for Phosphocholine Bilayers<sup>a</sup>

ID	charges/FF	DLPC	DMPC	DOPC	POPC	DPPC
1	Chiu/54A7	0.608(4)	0.591(4)	0.600(5)	0.604(4)	0.616(4)
2	Chiu/54A8	0.626(5)	0.612(4)	0.623(4)	0.623(4)	0.635(5)
3	RM/54A8_v1	0.631(4)	0.616(5)	0.625(6)	0.629(5)	0.638(5)
4	RM/54A8_v2	0.652(5)	0.643(6)	0.649(5)	0.650(5)	0.657(5)
5	RM/54A8_v3	0.690(6)	0.684(6)	0.690(6)	0.687(6)	0.693(5)
0	RM/54A7					0.603(5)
RF	Chiu/54A7					0.603(4)
small	Chiu/54A7					0.594(11)
experimental <sup>b</sup>		0.608–0.632	0.589–0.660	0.674–0.725	0.643–0.683	0.570–0.717
CHARMM36 <sup>37</sup>		0.644(4)	0.608(2)	0.690(3)	0.647(2)	0.629(3)

<sup>a</sup>The number in parentheses is the standard deviation of the last digit. All simulations are run at 303 K, except for DPPC (run at 323 K). Analogous values for POPE and POPG are reported in SI Tables 6 and 8. <sup>b</sup>We report the maximum and minimum values of a review of experimental results given in Table 1 of ref 74. Only values referring to the temperature simulated are considered.

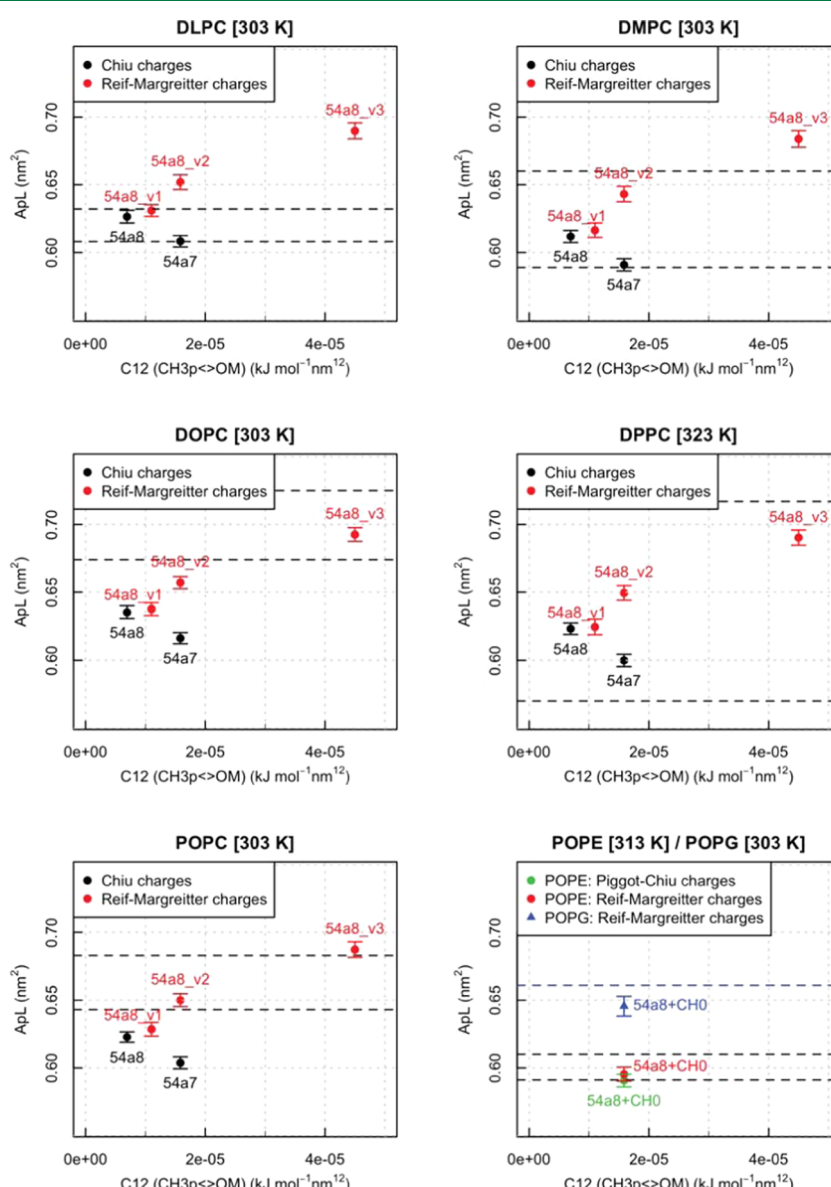


**Figure 3.** Area per lipid obtained for the five sets of parameters and seven lipid species. Error bars are the standard deviation over the 300 ns analyzed. Dashed lines indicate the range of experimental values from Table 1 in refs 74 and 33. For the plot reporting POPE and POPG values, the black dashed lines refer to POPE and the blue one to POPG.

2.5.8. *Lateral Diffusion.* For each simulation, we extracted the trajectory of the phosphorus atom of every lipid in the top and bottom leaflets separately, removing the collective motion of the leaflet. These trajectories were used to compute the mean-square displacement (MSD) for each lipid as a function of time, discarding the first 200 ns of production. This figure was averaged over all of the lipids in the leaflet and, for a given interval of time, on all of the possible time windows of that length-fitting within the simulation time analyzed. The diffusion coefficient  $D$  was obtained from a linear fit of the average MSD profile, following the Einstein equation<sup>79</sup> in two dimensions

$$\langle (x - x_0)^2 \rangle = 4Dt \quad (6)$$

The fit was performed discarding the first 50 ns of the profile, where the behavior is not linear, and the last 100 ns, where the poorer statistics leads to more noisy data. Coefficients obtained for the two leaflets were averaged to give the value reported.

2.5.9. *Tilt Modulus.* We computed the tilt modulus following the theoretical framework explained in ref 80. According to this, the angle  $\theta$  a lipid forms with the local normal to the membrane follows the distribution

$$P(\theta) = C \sin(\theta) \exp\left(-\frac{\kappa_t^1 \theta^2}{2k_B T}\right) \quad (7)$$

where  $C$  is a normalization constant,  $k_B$  is the Boltzmann constant,  $T$  is the temperature, and  $\kappa_t^1$  is the tilt modulus. This can be extracted from a fit of the distribution or, for computational reasons, from a fit of  $\ln(P(\theta)(\sin \theta)^{-1})$ . The direction in which a lipid points is taken as the vector joining the center of mass of the terminal atoms of the tails and the center of mass of selected atoms in the head group. Specifically, the last three carbons of each tail are taken as the reference for the first group, and the phosphorus and the carbon from which the two tails divert for the second. The computation was performed using a dedicated python module<sup>80</sup> available on the openStructure platform.<sup>81</sup>

**2.6. Phase Transition.** The set of new parameters performing best according to the previous observables was tested for sensitivity to temperature variations. A DPPC bilayer was chosen as the reference system and simulated at two additional temperatures: 303 and 333 K (SI Table 1), the first of which is below the experimentally determined liquid to gel phase transition temperature.<sup>63–66</sup> As DPPC has also been used to perform the other control simulations, we opted for this model membrane for consistency reasons.

Besides the standard analysis described before, the local area per lipid was computed using a Dirichlet tessellation<sup>82</sup> of the lipid head positions projected onto the horizontal plane parallel to the membrane (one leaflet at the time). The tessellation divides the plane into polygons, each enclosing one head position. Every polygon comprises the locations on the plane, which are closer to the position of the head enclosed by that polygon than to any other heads.

Moreover, to quantify whether and how many lipids undergo face transition during the simulations, the regular packing of each of their chains was quantified by the hexagonal order parameter  $S_6$ , as previously reported in the literature.<sup>83</sup> Specifically, a chain was represented by its position on the  $xy$  plane (parallel to the membrane surface), computed as the average  $x$  and  $y$  positions of its carbon atoms. For each chain  $j$ ,

the set of neighboring chains was defined as the ones within a 0.65 nm radius from  $j$ . Then,  $S_6$  is defined as

$$S_{6,j} = \frac{1}{6} \left| \sum_k e^{6i\theta_{jk}} \right| \quad (8)$$

with  $\theta_{jk}$  being the angle between the vector connecting  $j$  and  $k$  and the  $x$  axis ( $i$  is the imaginary unit). A chain is in the gel phase if it has an hexagonal order parameter larger than 0.72.<sup>83</sup>

### 3. RESULTS AND DISCUSSION

In general, the parameters described in this work are shown to reproduce the available experimental target values well while, at the same time, are likely to allow for a better description of lipid–protein interactions, since the head groups are updated to the recent GROMOS force field.

**3.1. Area per Lipid and Isothermal Area Compressibility Module.** We report in Table 3 and Figure 3 the values of ApL for the simulation run. From such computations, it emerges that the increase of the CH3p–OM repulsion has a nonlinear effect on the area per lipid, as reported in ref 54. On the contrary, the comparison between simulation ID1 and the control ID0 for DPPC, which differ only in their partial charges, shows an almost identical ApL value (SI Figure 4). This suggests that the charge redistribution in the head group affects the global structure of the bilayer and the ApL less dramatically than the adopted value for the Lennard-Jones repulsion.

The comparison with the control simulation using a smaller membrane shows that larger systems allow for the evaluation of the ApL with a smaller error, as local fluctuations are averaged over a larger number of lipids. The standard deviation computed for the 128-lipid system is compatible with those reported in both the original<sup>58</sup> and a more recent publication,<sup>84</sup> in which the same system size was used.

The ApL from the simulation with a reaction field treatment for the long-range electrostatic term does not differ significantly from the one obtained with a PME treatment, being only slightly higher, which is in consistence with what was found in ref 85.

Finally, the values found using the Chiu charge set and the S4A7 force field (ID1 in Table 1) are systematically lower than those obtained in the original publications,<sup>44,58</sup> despite employing the same charge set and force field, while a better agreement is shown with those obtained more recently by Reif et al. for DPPC.<sup>54</sup> We attribute this to the different versions of GROMACS used, as the integration algorithm has recently been updated, affecting the calculated properties. Moreover, the double-cutoff scheme is no longer supported, preventing a faithful reproduction of the simulation setup used in ref 58. The variability caused by these changes has been extensively investigated by Reißen et al.<sup>84</sup> and reflects the observed discrepancy between the present and previous results.

From the considerations above, we suggest parameter set RM/S4A8\_v1 as the one that best reproduces all of the tested lipids at once. For DOPC and POPC bilayers, however, parameter set RM/S4A8\_v2 performs slightly better: it must be noticed that these two species present unsaturated bonds along the tails, whose influence might not be fully represented by any of the parameter sets. Indeed, it has been suggested that only a polarizable force field would be able to correctly capture the dynamics of the hydrophobic region of the membranes,<sup>86</sup>

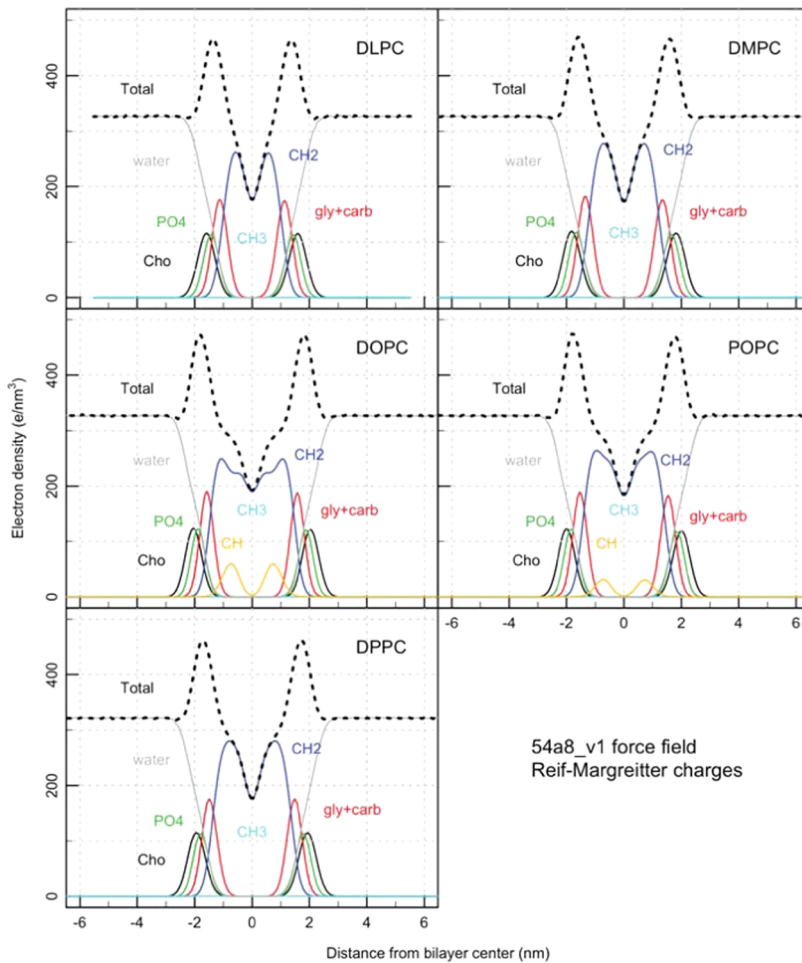


**Figure 4.** Electron density profiles of the hydrated DLPC, DMPC, DOPC, DPPC, and POPC bilayers (total) and of their individual components (Cho: choline, PO4: phosphate, gly + carb: glycerol and carbonyl groups, CH2: methylenes of the acyl chains, CH: CHdCH groups in the oleoyl chains, CH3: terminal methyls of the acyl chains) for simulation ID3 (S4A8\_v1 force field, Reif–Margreitter charges).

**Table 4. Bilayer Thickness for Phosphocholine Bilayers, Derived from the Electron Density Profiles (Example in Figure 4) According to the Phosphate or Luzzati Methods<sup>a</sup>**

hydrophobic thickness $D_{\text{HH}}$ (nm)						
ID	charges/FF	DLPC	DMPC	DOPC	POPC	DPPC
1	Chiu/S4A7	2.83	3.59	3.05	3.30	4.30
3	RM/S4A8_v1	2.72	3.48	2.89	3.22	4.06
experiment <sup>b</sup>		3.08	3.44–3.60	3.53–3.71	3.70	3.42–3.83
Luzzati thickness $D_B$ (nm)						
ID	charges/FF	DLPC	DMPC	DOPC	POPC	DPPC
1	Chiu/S4A7	3.11	3.54	4.13	4.00	3.93
3	RM/S4A8_v1	3.04	3.48	3.94	3.88	3.75
experiment <sup>b</sup>		3.14	3.63–3.96	3.59–3.87	3.68	3.50–3.83

<sup>a</sup>All simulations were run at 303 K, except for DPPC (323 K). <sup>b</sup>Values from ref 44 and Table 2 in ref 58.

taking in proper account the difference between saturated and unsaturated bonds.

For POPE and POPG, we resorted to the modification proposed by Kukol,<sup>46</sup> i.e., the use of the CH0 atom type for the ester carbons (see Section 2). For both lipids, a good agreement with experimental ApL values could be achieved using the new partial charge parameters (Figure 3).

Along the same lines, when comparing the results with the ones obtained with the CHARMM36 force field in its original publication,<sup>62</sup> we find DOPC, presenting an unsaturated bond

in each tail, to be the most diverging. In particular, CHARMM36 better captures the spacing between the lipids, enhanced due to the presence of the double bond, and we suspect that this is due to its all-atom description.

Results of the isothermal area compressibility calculations confirm the finding of refs 58 and 62 that  $K_A$  values obtained from simulation are about 1.5–3 times larger than those measured experimentally (SI Table 3). This holds for all parameter sets tested. Set RM/S4A8\_v1 performs better than

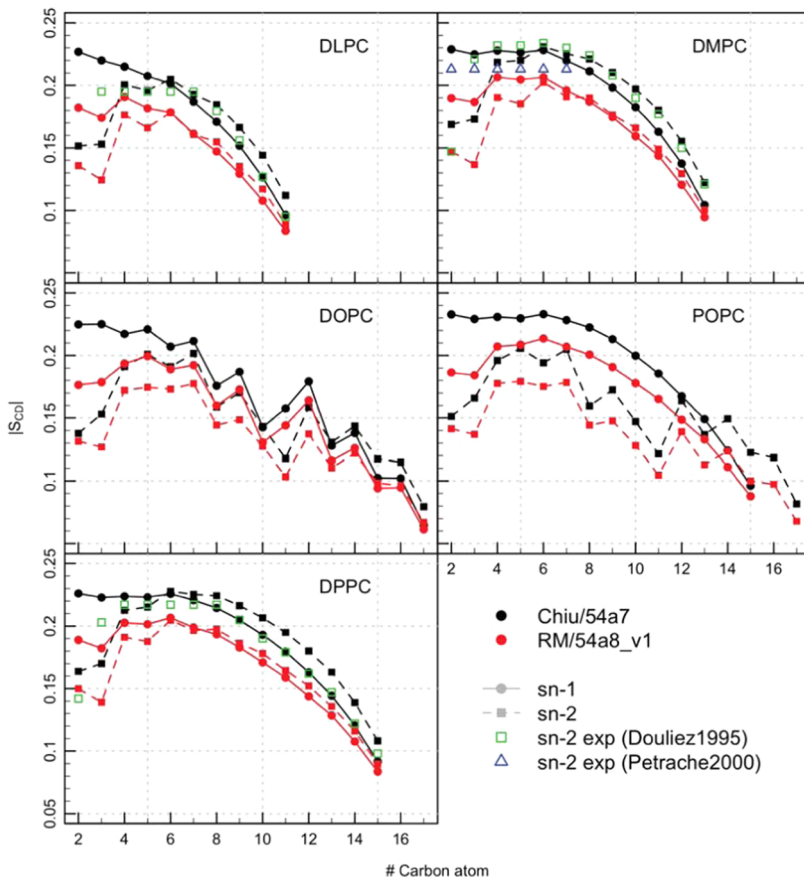


**Figure 5.** Deuterium order parameter  $S_{CD}$  profiles of the  $sn\text{-}1$  (solid curves) and  $sn\text{-}2$  (dashed curves) fatty acyl chains of hydrated DLPC, DMPC, DOPC, DPPC, and POPC bilayers calculated from simulations ID1 (54A7 force field, Chiu charges) and ID3 (54A8\_v1 force field, Reif–Margreitter charges). The  $S_{CD}$  values are averaged over all of the lipid  $sn\text{-}1$  and -2 acyl chains in the systems. Experimental values Douleuz1995 from ref 89 and Petrache2000 ones from ref 90.

571 Chiu/54A7 for all of the lipids tested but DLPC, for which the  
572 results are equivalent.

573 The overestimation of the compressibility is likely due to the  
574 underestimation of ApL fluctuations during dynamic simu-  
575 lations. The  $K_A$  value computed for the small, 128 lipids,  
576 DPPC bilayer patch is smaller than the one computed for the  
577 512 lipid ones (342 and 499 mN m<sup>-1</sup>, respectively), as the  
578 small patch exhibits higher fluctuations of the ApL (see Section  
579 3.1). It is thus evident that the size of the system plays a pivotal  
580 role in obtaining correct fluctuations and global properties.

581 **3.2. Electron and Charge Density Profile.** Across  
582 simulations with different parameters, the electron density  
583 qualitatively maintains the same profile for each phosphocho-  
584 line lipid. In Figure 4, the density for parameter set 54A8\_v1  
585 and all of the lipids is displayed (SI Figures 10–13 show the  
586 same plot for the other parameter set), while in SI Figures 5–  
587 9, panel (b), the total and the phosphate group electron  
588 densities are shown for the five parameter sets tested, for one  
589 lipid at the time. The peak broadness shows a direct  
590 relationship with the packing density of the bilayer: larger  
591 ApL values correspond to a shallower profile of the density,  
592 due to fluctuations of the membrane along the  $z$  axis and to  
593 deeper penetration of water molecules into the bilayer.

594 The bilayer thickness was evaluated from the electron  
595 density profiles, as explained in Section 2. Our parameters are  
596 overall in better agreement with the Luzzati estimate of the  
597 thickness rather than the hydrophobic one, but altogether,  
598 these measurements (phosphate and Luzzati thickness) do not

599 strongly discriminate between sets. In Table 4, the values for 599 t4  
the Chiu/54A7 and RM/54A8\_v1 sets are shown (see SI 600  
Table 4 for the complete results).

601 Further comparison of the dipole potential profiles, obtained 602  
from the charge density, shows how the RM/54A8\_v1 charge 603  
set gives results closer to the ones obtained in all-atom 604  
simulations<sup>77,87</sup> (see SI Section 1 for a complete discussion).

605 **3.3. Order Parameter of the Acyl Chains.** For all of the 606  
lipids and parameter sets,  $S_{CD}$  is lower than 0.25, which 607  
indicates that the tails are generally disordered and the 608  
membrane has not transitioned to a gel-like state,<sup>88</sup> even for 609  
the simulation with the lowest ApL. Figure 5 and SI Figures 609 f5  
14–17 display the computed values for specific parameter sets,  
611 and SI Figures 5–9, panel (c), show a cross-parameter 612  
comparison for each lipid. Comparing these different sets,  
613 simulations denoted by ID from 1 to 5 show a consistently 614  
decreasing  $S_{CD}$ , in line with the increased area per lipid and 615  
decreased bilayer thickness. This indicates that when the lipid 616  
molecules are constrained in space, their tails tend to be 617  
stretched and ordered. The presence of unsaturated bonds in 618  
the DOPC and POPC lipids is captured, by all parameter sets,  
619 as a decrease in  $S_{CD}$  at the positions related to those bonds.  
620 The main difference due to the introduction of the new 621  
charges is in the decreased order observed for the first and 622  
second carbon bonds of the  $sn\text{-}1$  tail, which show  $S_{CD}$  values 623  
smaller than the ones for the third carbon bond, while with the 624  
Chiu charges, a constant increase is observed with decreasing 625  
carbon index for tail  $sn\text{-}1$ .

Overall, the RM/S4A8\_v1 set is within the range of experimental values<sup>89,90</sup> (Figure 5); in particular, it captures the low order of the first *sn*-2 carbon atom (numbered 2) well, while the Chiu/S4A7 set presents closer values in the central region of the tails. However, it must be noticed that variability is found within the experimental data (see the different experimental values reported in Figure 5). Therefore, without aiming at a perfect fit to such a small pool of experimental data, we consider set RM/S4A8\_v1 as sufficiently accurate in representing the experimental findings, in particular, in better reproducing the regions in the vicinity of the head group, while the description of the hydrophobic core remains less accurate and subject to improvement.

**3.4. Hydration of Head Groups and Glycerol/Carbonyl Moieties.** The hydration of functional groups of lipids is a key characteristic for both their dynamics and potential interactions with other molecules, such as proteins. From the distribution of distances between water oxygens and the nearest atom of various lipid groups, it emerges that the new partial charges modify the hydration profile of the lipid head group (Figure 6 shows the comparison between parameter sets for DPPC and SI Figures 17–20 for the other lipid bilayers).

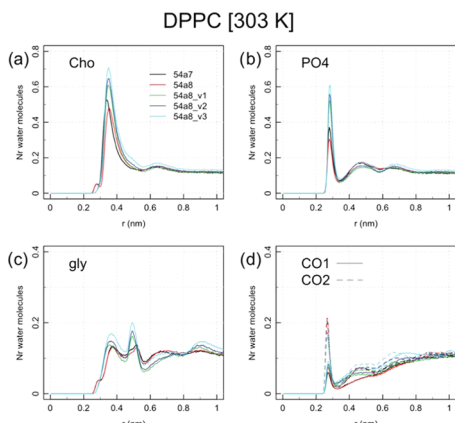


**Figure 6.** Distribution of the distance between the water oxygen and the nearest lipid head group atom for simulation DPPC. Cho: choline, PO4: phosphate, Gly: glycerol, CO1 and CO2: carbonyl groups at the *sn*-1 and *sn*-2 positions.

The choline major peak at 0.38 nm and the phosphate one at 0.30 nm are higher and sharper when employing the RM charges rather than the Chiu ones, reflecting an increased average hydration of these two moieties. Additionally, for the simulations run with the RM charges, the choline profile does not display the first, low intensity, peak obtained with the Chiu set at 0.28 nm: indeed, the charges of choline and the modification of the C12 Lennard-Jones repulsion for the NL

atom type introduced in parameter set S4A8 were optimized to successfully prevent oversolvation, repelling water from its core.<sup>47,54</sup> The profiles of the other components are partially influenced, as well. For the RM charges, the second peak for glycerol increases its value and the two ester peaks have more similar values between them (Figure 6, panel (c), and SI Figures 17–20), which is consistent with deeper water penetration.

To quantify the observed differences, the hydration profiles were integrated up to the first peak or the second one in the case of phosphate and glycerol (SI Table 5). The results show that the average number of water molecules around the choline group is higher for the RM/S4A8\_v1 set than for the Chiu/S4A7 one by one water molecule. This seems to contrast with the increased hydrophobicity of the newly parameterized choline moiety; however, this might partially be explained by the changed orientation of the head groups (see Section 3.5) and by the new parameterization of phosphate,<sup>48</sup> which accounted for the hydrogen bond potential of the most solvent-accessible atoms, leading to a better solvation of the head group in comparison to the Chiu/S4A7 and Chiu/S4A8 sets.

The integration up to the second peak of the distribution of distances between the water oxygens and any lipid head group atom gives values between 12 and 17 water molecules per lipid, which is in agreement with the experimental range of 10–20.<sup>91–94</sup> Again, parameter set RM/S4A8\_v1 results in more hydrated head groups (about one water molecule more for each lipid) with respect to Chiu/S4A7. Notably, the average number of water molecules increases, as expected, for the simulations resulting in a larger ApL (RM/S4A8\_v2 and RM/S4A8\_v3). The trends above are confirmed by solvent-accessible surface area values, which are higher for the choline head groups described by the RM charge set with respect to the Chiu one, while the values are closer between parameter sets for the phosphate and glycerol moieties, which are more deeply buried (SI Figure 21).

The increased hydration might be of relevance when simulating interactions with peptides and proteins. Moreover, as shown in a recent comparison between different lipid force fields,<sup>62</sup> the Chiu/S4A7 parameter set results in a slightly less hydrated head group with respect to the CHARMM36 and Lipid14 force fields; therefore, the new set of parameters achieves values closer to them.

**3.5. Orientation of the Head Groups and Carbonyl Moieties.** The orientation of the head groups, defined by the angle of the P–N vector with the outward bilayer normal, is similar for all of the lipids within the same parameter set (see SI Figure 22, top row). This indicates that the nature of the tails does not strongly affect the behavior of the head group, which is to be expected. Comparing different sets for DPPC

**Table 5. Binding Time of Lactoferricin (LFC) Peptide to the Model Membranes in Examination<sup>a</sup>**

	binding time (ns)							
	DLPC/DLPG 3:1				POPC			
	OI	OII	OIII	OIV	OI	OII	OIII	OIV
Chiu/S4A8	0.5	3.8	6.3	2.8	13.9	21.9	(65.0)	13.9
RM/S4A8_v1	2.8	75.2	62.0	9.6	1.0	NA	NA	NA

<sup>a</sup>NA denotes no binding observed in the time simulated (100 ns). For POPC/OIII simulated with parameter sets Chiu/S4A8, the binding time is in parentheses as LFC approaches the membrane but maintains a 0.4 nm distance ( $\pm 0.02$ ), which is higher than the threshold chosen to define a binding event.

708 (Figure 7 and SI Figure 23), it emerges that with the Chiu  
709 charges, the distribution of P–N angles is bimodal, with

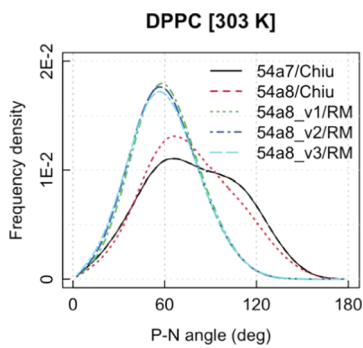


Figure 7. Distribution of the P–N, CO1, and CO2 angles with respect to the outward normal to the bilayer.

710 preferred values around 60 and 90°, while the new charges  
711 restrict the motion to the 60° configuration. Recent  
712 experimental data support a value around 60° (see refs 95  
713 and 96), as opposed to 90° as reported previously.<sup>97</sup>

714 It is noteworthy that this property was not part of the  
715 calibration process, i.e., the agreement with the experimental  
716 observables in ref 96 is most likely due to a more accurate  
717 description of the solvation of the choline and phosphate  
718 moieties. Simulations performed by Botan et al.<sup>98</sup> confirm that  
719 smaller angles with respect to the membrane normal are caused  
720 by a higher level of head group hydration, which is in line with  
721 conclusions from the previous section. This difference in the  
722 predominant configuration of the lipids' head group will most  
723 probably influence the interaction with proteins or peptides  
724 approaching the interfacial region, providing a different  
725 binding recognition landscape.

726 The orientation of the *sn*-1 and *sn*-2 carbonyl dipoles with  
727 respect to the bilayer normal is again similar across different  
728 lipids (SI Figure 22, middle and bottom rows). The  
729 introduction of the RM charges has a small effect on these  
730 dipoles, as a result of the spatial rearrangement of the nearby  
731 head group. The most probable value for CO1 is shifted from  
732 110 to 120° (Chiu vs RM charges), while the one for CO2  
733 from 135 to 150°.

734 **3.6. Lipid Lateral Diffusion.** To correctly reproduce the  
735 membrane and its functions, its dynamical characteristics are as  
736 important as its structural ones. To address this, lipid lateral  
737 diffusion can be measured and compared against experimental  
738 data. Lateral diffusion is influenced by the area per lipid, with a  
739 tighter packing preventing larger displacements but is not  
740 solely determined by it.

741 Lateral diffusion coefficients ( $D$ ) measured from simulations  
742 are shown in Figure 8. As anticipated, the set with largest ApL  
743 (54A8\_v3) presents the highest values; however, parameter set  
744 54A8\_v1 gives significantly higher diffusion coefficients than  
745 those obtained with the Chiu/54A7 set, despite the values of  
746 ApL being similar. SI Figure 24 depicts a comparison of the  
747 diffusion coefficient of DPPC between ID0 and ID1, which  
748 differ only in the partial charges of the head groups. This  
749 confirms that the RM charges (ID0) allow for more mobility of  
750 the lipids with respect to Chiu ones (ID1), independent from  
751 all other modifications to the force field.

752 Regarding the simulation conditions, the use of a reaction  
753 field scheme increases the mobility by 34%, whereas the size of  
754 the patch decreases it by a small but significant amount (19%;

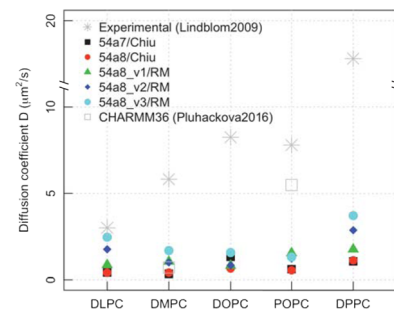


Figure 8. Lateral diffusion coefficient of DLPC, DMPC, DOPC, DPPC, and POPC bilayers for different parameter sets.

see SI Figure 24). It is known that periodic boundary conditions affect the evaluation of lipid diffusion;<sup>99,100</sup> therefore, the larger the system simulated, the more accurate the reproduction of the experimental values. However, the change in the  $D$  due to the electrostatic treatment and the patch size, taken in absolute terms (i.e., a difference of about 0.4 and 0.2  $\mu\text{m}^2 \text{s}^{-1}$ , respectively), are small in comparison with the effect due to the adoption of the new parameters (between 2 and 6  $\mu\text{m}^2 \text{s}^{-1}$ ).<sup>763</sup>

The comparison with experimental values is challenging due to the fact that different experimental techniques report values, which are an order of magnitude apart. Poger et al. gave an overview of this variability for DPPC bilayers in Table 2 of ref 74 and observed that values span from 0.5 to 50  $\mu\text{m}^2 \text{s}^{-1}$ . In this view, the values obtained in the present work for DPPC are well within the range, regardless of the parameter set chosen. However, we report experimental values from ref 101 obtained through pulsed-field gradient nuclear magnetic resonance as a guide. Additionally, we report the values obtained with CHARMM36 in ref 62. The CHARMM36 benchmarks are present only for two of the phosphocholines analyzed in this work and show that the values obtained with this force field span a broader range. The consistently low values of  $D$  computed with the different GROMOS parameter sets in this work are in agreement with what was found in the literature.<sup>102,103</sup>

**3.7. Tilt Modulus.** We report in Figure 9 the values of  $\kappa_t^1$  obtained for each of the phosphocholines considered and each parameter set tested. For comparison, we plot the experimental values obtained by Nagle et al. in ref 104 and the results from simulations using the CHARMM36 force field.<sup>105</sup> Given that the data show quite a large spread in their values depending on

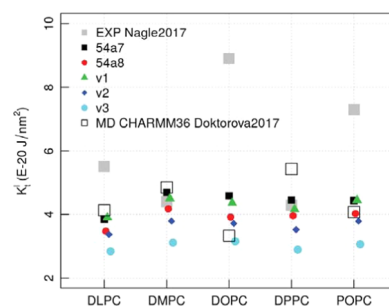


Figure 9. Tilt modulus  $\kappa_t^1$  computed from the distribution of lipid tilt angles along the last 300 ns of the trajectories. The results are compared with the experimental values from ref 104 and the ones obtained (with the same procedure as employed here) from CHARMM36 simulations in ref 105.

787 the actual experimental setup used, for the comparison, we  
 788 selected values, which were all obtained under the same  
 789 conditions, for both the experiments and the computational  
 790 results.

791 The plot shows that the tilt modulus  $\kappa_t^1$  varies between 3 and  
 792  $5 \times 10^{-20} \text{ J nm}^{-2}$ . In simulations resulting in larger ApL (e.g.,  
 793 parameter set S4A8\_v3), the lipids are in a less dense  
 794 environment and can better accommodate changes in their  
 795 orientations resulting in a lower tilt modulus (the tilt modulus  
 796 gives the energy necessary for tilting the lipids per unit area).

797 The comparison with the experimental values is very good  
 798 for DMPC and DPPC, while it is poorer for DLPC and very  
 799 poor for DOPC and POPC, which harbor unsaturated bonds  
 800 in the tails. Results from the CHARMM36 simulations show  
 801 more variability between different phosphocholines, but a  
 802 similar if not lower agreement with the experiment (for  
 803 example, for DOPC). In general, comparing the results  
 804 together, we think that we achieved a sufficiently qualitative  
 805 agreement with the previous computational literature.

806 The discrepancy with experiments (both for our results and  
 807 for the ones from ref 105) is likely due to computational  
 808 limitations: as the tilt is retrieved from an ensemble  
 809 distribution, larger and longer simulations are more likely to  
 810 give a better result. Moreover, as briefly mentioned at various  
 811 points in the manuscript, artifacts arising in the hydrophobic  
 812 regions of lipids (such as the suboptimal modeling of  
 813 unsaturated tails) will probably only be resolved using a  
 814 polarizable description.

815 **3.8. Phase Transition Behavior.** The previous analysis  
 816 points to parameter set S4A8\_v1 as the one that best  
 817 reproduces the experimental properties for each of the lipids  
 818 simulated. Therefore, we test this set further to assess its ability  
 819 to reproduce the change in lipid behavior under different  
 820 temperature conditions. As mentioned in Section 2.6, we use  
 821 as test system the DPPC bilayer patch.

822 The comparison between simulations at 323 and 333 K  
 823 shows that the global area per lipid increases with temperature,  
 824 consistently with what was expected. Parameter set S4A8\_v1  
 825 captures the increase in lipid spacing, with a slight under-  
 826 estimation of ApL at 333 K with respect to the experiments  
 827 (for S4A8\_v1 and experiments, respectively: 0.624(6) vs  
 828 0.631(13) nm<sup>2</sup> at 323 K and 0.634(5) vs 0.650(13) nm<sup>2</sup> at 333  
 829 K). The experimental ApL is measured at a different  
 830 temperature with the same experimental setup.<sup>16</sup>

831 The simulation at 303 K shows the formation of a patch of  
 832 ordered lipids, suggesting that the parameters can reproduce  
 833 different phases: two nucleation sites for the gelification  
 834 process are observed in both the upper leaflet and lower leaflet,  
 835 in nonmatching positions, and the gel front extends over time.  
 836 To classify the phase a lipid belongs to, we computed the  
 837 hexagonal order parameter  $S_6$  for each chain from the last  
 838 frame of the simulation (time point 400 ns). Figure 10 shows  
 839 the position of the chains on the xy plane, for each leaflet  
 840 separately, color-coded by  $S_6$ : the regions where  $S_6$  is larger  
 841 correspond to a densely packed area with a quasi-hexagonal  
 842 lattice. In particular, the center of the ordered patches has  $S_6$   
 843 values larger than 0.72 (last two colors of the scale), i.e., it can  
 844 be classified as a gel. Overall, 20% of chains have undergone  
 845 this transition within the time simulated.

846 Averaging over all of the lipids,  $S_6$  at 303 K is 0.45. As a  
 847 comparison, we computed this average quantity on the last  
 848 frame of the simulations performed at 323 and 333 K, finding

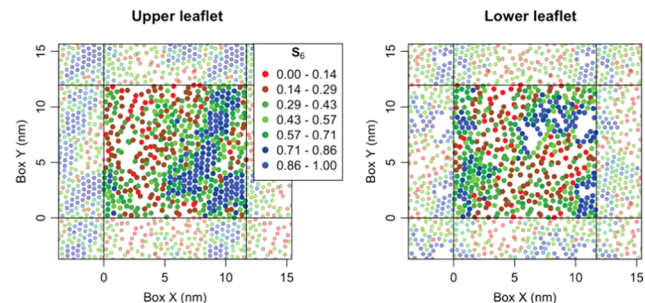


Figure 10. Hexagonal order parameter  $S_6$  for lipid acyl chains computed on the last frame of a DPPC bilayer simulation using S4A8\_v1 parameters. Each point corresponds to the average position of the carbon atoms of the respective chain on the xy plane. Thus, every lipid is represented by two points in these plots. Solid black lines denote the boundaries of the simulation box and chains of the periodic images (used for the computation of  $S_6$  boundaries) are shown faded out. Colors from red to blue denote an increasing  $S_6$  value: the last two indicate gel-phase lipids.

0.28 and 0.27, respectively (with only six and three chains above the gel threshold of 0.72).  
 849  
 850

A hexagonal order can be obtained when the tails are well  
 851 ordered and parallel to each other, standing in a vertical  
 852 straight conformation (SI Figure 25 shows a detail of a well-  
 853 ordered gel patch). We thus compute the  $S_{CD}$  order parameter  
 854 of the acyl chains averaging separately over the lipids for which  
 855 at least one chain has an  $S_6$  value larger than the 0.72 threshold  
 856 (168 lipids overall) and for the others. The last 100 ns of the  
 857 simulation time was used. These values are compared to the  
 858 average  $S_{CD}$  from the simulations at 323 and 333 K. Figure 11  
 859 f11

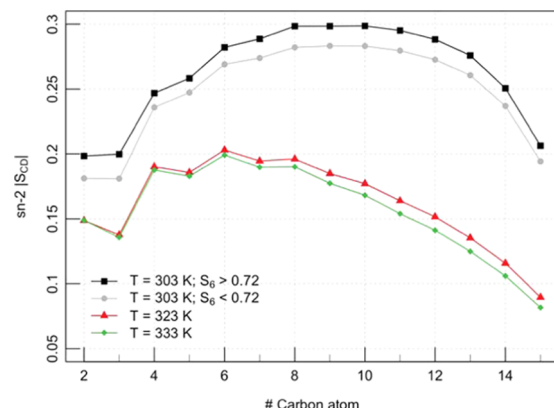
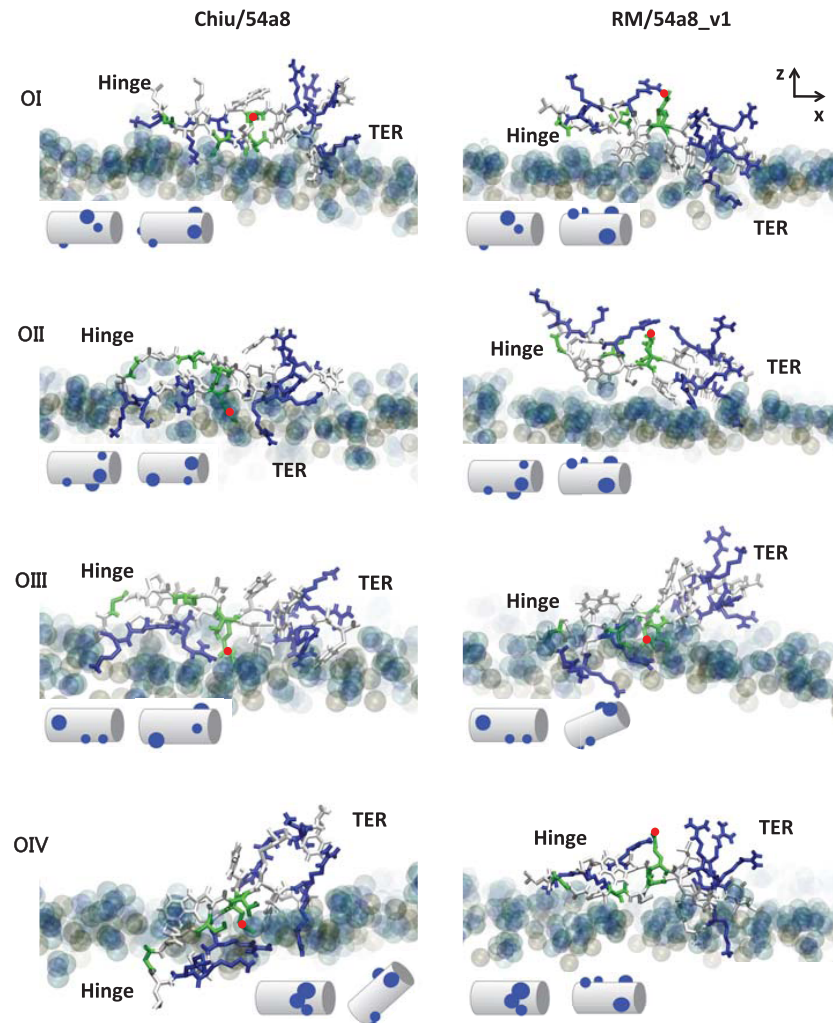


Figure 11. Order parameter for the acyl chain sn-2 for a DPPC bilayer simulated at a different temperature. The average is performed including both leaflets. For the simulation at 303 K, the lipids were split in two groups according to their hexagonal order parameter  $S_6$  and the acyl chain order parameter  $S_{CD}$  computed for each of them.

shows highly ordered tails for the membrane simulated below  
 860 the transition temperature, for both the gel and nongel lipids  
 861 (classified according to the  $S_6$  threshold). This suggests that  
 862 the full patch is undergoing a phase transition, but the  
 863 completion of the process is not seen due to the short  
 864 simulation time scale. As a comparison, tails at 323 and 333 K  
 865 are much more disordered, with a slight decrease in order with  
 866 increasing temperature.  
 867

Finally, we computed the local area per lipid chain from a  
 868 Dirichlet tessellation of the same set of points used to calculate  
 869



**Figure 12.** Final configurations of the simulations of LFC on a DLPC/DLPG 3:1 membrane, starting from four different initial orientations OI–OIV. OII, OIII, and OIV are obtained from OI with an anticlockwise rotation of, respectively, 90, 180, and 270° along the main axis ( $x$  axis in the top right panel). LFC is colored by residue type (blue charged, green hydrophilic, white hydrophobic); phosphorus atoms are shown in golden beads. The terminal and hinge regions of 1LFC are indicated (TER, hinge), together with GLN7 as a red dot to help the visualization. The insets shows a cartoon representation of the initial and final configurations, highlighting the positive patches as blue dots.

the hexagonal order parameter. The average values over the gel-phase tails (multiplied by 2) give an  $A_pL$  of  $0.438 \pm 0.038 \text{ nm}^2$ , while the remaining of the chains have widely spread values, correlated to their  $S_6$  parameter, giving an average of  $0.57 \pm 0.18 \text{ nm}^2$ . The values found for the gel patches (at 303 K) are close to the experimental outcomes by Nagle et al. of 0.473 nm $^2$  at 293 K<sup>106</sup> and 0.479(2) at 297 K.<sup>107</sup> The value computed from simulations is smaller likely because it is computed only over the tails perfectly packed in a hexagonal lattice.

Altogether, these results prove that the newly developed parameters can successfully reproduce the gel phase when a lipid patch is simulated below the phase transition temperature.

**3.9. Transferability to POPE and POPG.** As mentioned above, the areas per lipid values of POPE and POPG simulations, where the phosphate partial charges have been replaced with the RM values and, in the case of POPE, the amine partial charges have been updated according to the 54A8 force field, are in good agreement with the available experimental data.

For POPE, a slightly enhanced hydration is obtained from the update of the phosphate charges (from 5.7 to 6.4 water molecules per lipid with experimental values between 4 and 7;<sup>108,109</sup> see SI Table 7) with similar results in terms of thickness  $D_B$  (3.89 nm for Chiu and 3.92 for RM set, with an experimental value of 4.13 nm;<sup>110</sup> SI Table 6 and SI Figures 26 and 27). Overall, these results confirm the transferability of the new phosphate charges to different types of phospholipids.

#### 4. INTERACTION WITH PROTEINS

The adoption of the updated parameters enhances the consistency with the GROMOS parameters for protein simulations. To test how this affects the simulations of peptides interacting with a membrane, we performed additional simulations of a small antimicrobial peptide on the surface of two different model membranes.

The peptide selected is bovine lactoferricin (PDB code 1LFC). It has a length of 25 amino acids and adopts a  $\beta$ -hairpin conformation in solution, with many aromatic hydrophobic residues on one side and charged amino acids distributed all over.<sup>111</sup> This peptide is antimicrobial and therefore found to preferentially bind bacterial membranes

versus mammal ones, as shown by NMR experiments on LFC subsequences (namely, LFC<sub>4–9</sub><sup>112</sup> and LFC<sub>4–14</sub><sup>113</sup>).

One can model the bacterial membrane by a mixture of zwitterionic and anionic lipids. The latter are characteristic of the cell wall of both Gram-positive and -negative bacteria.<sup>114,115</sup> In this study, we selected the mixture DLPC/DLPG with a 3:1 ratio that has been used to elucidate the antimicrobial activity of lactoferricin-derived peptides.<sup>116</sup> As for the mammal membrane description, we used POPC as it has been often used in molecular dynamics simulations with this purpose.<sup>117–119</sup> Despite being rather simple, these or similar model membranes have often been used in experiments to test, among others, the effects of antimicrobial peptides upon binding.<sup>114</sup>

Molecular simulations can shed light on the differences in the binding process of LFC to antimicrobial and mammal model membranes. Our parameterization should then reflect a sensible difference in the binding behavior for these two cases.

The exact binding mechanism of LFC to a membrane is not fully understood, and a number of experimental papers have hypothesized binding modes for the interactions of this peptide with model membranes. A mutation study in LFC<sub>1–15</sub> suggests that Trp residues anchor the peptide to the membrane as the antimicrobial activity of the peptide was retained only when Trp was mutated in equally hydrophobic amino acids.<sup>120</sup> However, the role of Trp seems to be different in other antimicrobial peptides, where they reside at the lipid–water interface and form hydrogen bonds with the moieties nearby.<sup>121</sup> As experiments on the full-length peptide (25 amino acids) have not yet been reported and the full sequence contains additional charged and hydrophobic residues, it remains unclear whether this additional region would change the aforementioned binding mechanism. We therefore decided to use molecular dynamics simulations to elucidate molecular determinants in discriminating the binding of the peptide to mammal and bacterial membranes.

In order to not be biased by the initial configuration adopted in the simulation, we performed multiple simulations with different initial orientations of the peptide relative to the membrane. The hairpin main axis was aligned to the membrane plane and the peptide rotated around this axis in steps of 90°, leading to four different starting orientations named OI, OII, OIII, and OIV (SI Figure 29). This allows different segments of the sequence (and thus amino acids with different chemical characteristics) to face the membrane in the initial positioning. The initial minimum distance between the peptide and the lipids was set to 2 nm. The simulation length was 100 ns each, sufficient to see the binding process in all of the control cases.

The simulations have been performed for the proposed RM/54A8\_v1 parameter set and the Chiu/54A8 one (control cases) to compare with the most recent set available in GROMOS and highlight the difference of the newly parameterized lipid head groups.

To quantify the outcome of the simulations, we monitored the time at which the peptide binds (always irreversibly) to the membrane as the time at which the minimum distance between the peptide and the membrane is below 0.3 nm (Table 5). The cutoff was chosen, analyzing the configurations after LFC bound to the membrane, which resulted generally to stabilize around a minimum distance of 0.25 nm. The minimum distance was computed every 100 ps, and a running average was applied with a 10 frame window. Additionally, the

insertion depth of each amino acid in the membrane has been calculated as the difference between the *z* position of the lowest atom of the amino acid and the average of the maximum *z* coordinate of the five lipids closest to it.

Table 5 shows the different binding times for LFC against a mixed DLPC/DLPG or pure POPC membrane patch. For the mixed, anionic membrane, the new parameters favor a slower and weaker binding process. Indeed, with parameter set Chiu/54A8, the peptide is quickly sequestered by the lipids due to the opposite charge interaction. This favors an unspecific binding, dependent on the sequence facing the membrane in the initial configuration (Figure 12 and SI Movie 1). In Figure 13, the average insertion in the membrane after the binding is

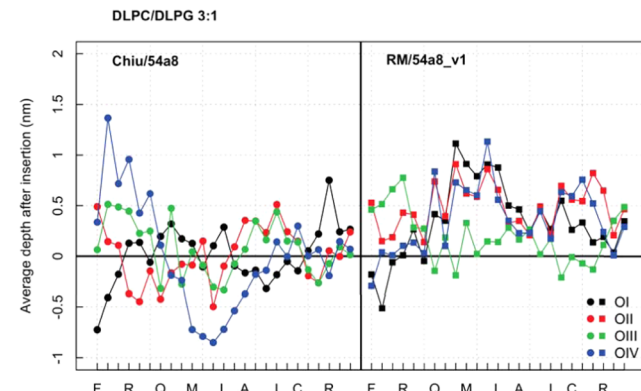


Figure 13. Average insertion depth of each amino acid after binding of the LFC peptide as per Table 5. The zero value is the top of the membrane plane so that a negative depth means insertion into the membrane. Some reference amino acids are displayed at the bottom.

plotted for each amino acid: Chiu/54A8 favors a deep insertion of differently charged residues for different runs. The RM/54A8\_v1 simulations produce a less inserted configuration of LFC and a more consistent protrusion of the hinge region out of the membrane, i.e., the central stretch of amino acids between Met and Leu (Figure 13), as three out of the four simulations (all but OIII) show this behavior.

The angular orientation of the peptide around its axis has been computed as the angle formed with the *z* axis by the backbone carbon and nitrogen bonded via a hydrogen bond (amino acids 7 with 19 and 9 with 17), confirming that the new set of parameters allows for more freedom in the reorientation of the initial configurations, while the previous one tends to keep them close to the original configuration (SI Figure 30). Additionally, the new set of parameters seems to favor the reorientation of the peptide as to face the Trp residues toward the membrane surface in three out of the four simulations, in contrast with the results from the previous parameterization. This preference for the interfacial region is a known mechanism in the membrane binding of Trp- and Arg-rich peptides.<sup>121</sup>

When simulating a pure POPC membrane (here considered as a mammal membrane model), the resulting binding poses obtained with the Chiu/54A8 and different initial conditions are consistent among each other; in particular, the three amino acids Lys12–Leu13–Gly14 located at the hinge of the hairpin promote the insertion, while the terminal region stays exposed in solution. Therefore, parameter set Chiu/54A8 discriminates between the two membranes as it suggests a weaker binding to the mammal one. However, with the parameter set RM/

1017 S4A8\_v1, three out of the four simulations result in no binding  
1018 at all, in agreement with experimental findings.<sup>112</sup> The  
1019 remaining simulation (OI) shows a quick binding event,  
1020 promoted by the terminal regions as observed for three out of  
1021 four simulations with the DLPC/DLPG 3:1 membrane.

1022 The results above highlight that the new parameters show a  
1023 membrane-binding process less dependent on the initial  
1024 conditions, allowing for a dynamical rearrangement of the  
1025 protein at the membrane interface. This comes at the expenses  
1026 of a longer sampling time needed to observe binding events for  
1027 most of the configurations chosen. Future work will focus on  
1028 systematic comparisons of available peptide–membrane  
1029 simulations with other parameterizations and on longer  
1030 simulated times.

1031 The difference between the behavior on a model bacterial or  
1032 mammal membrane is more pronounced for the new  
1033 parameters, and this is consistent with the selective  
1034 antimicrobial action of the peptide and its low hemolytic  
1035 activity.<sup>112,113</sup> Overall, we think that these new parameters  
1036 show promising characteristics for the simulation of mem-  
1037 brane–peptide interactions within the GROMOS force field,  
1038 particularly for the study of interfacial absorption.

## 5. CONCLUSIONS

1039 In this work, we present a reparameterization of a range of  
1040 phospholipids in the context of the GROMOS force field,  
1041 taking advantage of recent optimizations reported for key  
1042 chemical groups in these molecules. The effect of the newly  
1043 adopted head group partial charges has been tested extensively  
1044 to ensure that they match experimentally observable character-  
1045 istics of lipid bilayers. In parallel, we tested the effect of the van  
1046 der Waals repulsion between the choline methyl groups and  
1047 the phosphate oxygens, as it was modified by Poger et al. to  
1048 reproduce the experimental area per lipid values while using  
1049 the partial charges derived by Chiu et al. A summary of the  
1050 updated parameters and simulation conditions is available in SI  
1051 Table 10.

1052 The work proves that the new charges are suitable to  
1053 describe all of the phosphocholine bilayers tested, matching  
1054 the experimental values as successfully as the previous  
1055 parameter set. The major advantage of the Reif–Margreitter  
1056 set lies in the partial charges of the head group, which are  
1057 derived by applying the GROMOS parameterization philoso-  
1058 phy rather than quantum mechanics calculations, thereby  
1059 providing a description, which is more consistent with the  
1060 parameters adopted for other biomolecules such as proteins  
1061 within this force field. By using the updated partial charges for  
1062 the choline (more hydrophobic) and phosphate (more  
1063 hydrophilic) groups, the parameters also show a better  
1064 reproduction of the average head group orientation, which  
1065 was recently reassessed by experiments. The value of the  
1066 Lennard-Jones repulsion term found to best reproduce the  
1067 experimental values is the one in set S4A8\_v1, which is set to a  
1068 value in between that of the S4A7 and S4A8 parameter sets.

1069 In the Reif–Margreitter parameter set, only the partial  
1070 charges of the ester groups remain as described in the Chiu  
1071 charge set. Preliminary work has been started to test the  
1072 influence of the ester charges in combination with the new  
1073 ones for the head group but, in accordance to what was  
1074 previously found by Chandrasekhar et al. (ref 56), the  
1075 replacement of the ester charges with the standard ones for  
1076 the ester moiety resulted in values of area per lipid too low  
1077 with respect to the experimental findings. As mentioned

1078 previously, it is possible that this discrepancy with the rest of  
1079 the force field can only be avoided by adopting a polarizable  
1080 force field.<sup>86</sup> However, in the absence of further sophisticated  
1081 changes to the force field parameterization, we are confident  
1082 that the proposed parameters are a major step forward in the  
1083 description of lipid head groups and they should enable  
1084 improved modeling of the interaction of lipids with water and  
1085 other soluble molecules.

1086 The new phosphate partial charges have been proved to  
1087 transfer well to other phospholipids not presenting a choline  
1088 head. For those lipids, the Kukol modification, which takes  
1089 advantage of a different atom type for the ester carbon, is  
1090 adopted to obtain the correct area per lipid.

1091 Finally, the performance in reproducing some specific  
1092 peptide–membrane interactions was tested. In this respect,  
1093 the new parameter set shows significant differences with  
1094 respect to the latest Chiu/S4A8 set: it better discriminates the  
1095 binding of an antimicrobial sequence on a bacterial versus a  
1096 mammal membrane. Additionally, it favors a weaker and more  
1097 dynamic binding, which is less biased from the initial  
1098 conditions of the simulations.

1099 In conclusion, we believe that the new Reif–Margreitter  
1100 charge set together with the GROMOS S4A8\_v1 parameter set  
1101 is a major improvement on the previous iteration of the  
1102 GROMOS lipid force field and should be particularly suited for  
1103 protein–membrane systems, such as studies including small  
1104 antimicrobial peptides, which rely on an accurate peptide–  
1105 membrane recognition.

## ■ ASSOCIATED CONTENT

### S Supporting Information

1106 The Supporting Information is available free of charge on the  
1107 ACS Publications website at DOI: 10.1021/acs.jctc.9b00509.

1108 Additional control simulations; simulations for POPE  
1109 bilayer; compressibility values for PC lipids; thickness  
1110 values for PC lipids; lipid moiety for PC lipids, POPE  
1111 and POPG bilayers; properties of POPE and POPG  
1112 bilayers; previous parameters and simulation setup (SI  
1113 Tables 1–10); dipole potential; time series of the ApL  
1114 for a DPPC bilayer; ApL for different time windows of  
1115 the same simulation and control simulations; compar-  
1116 ison of key properties across parameter sets for DLPC,  
1117 DMPC, DOPC, POPC, and DPPC bilayers; electron  
1118 density profiles of bilayers for parameter sets Chiu/  
1119 S4A7, Chiu/S4A8, RM/S4A8\_v2, and RM/S4A8\_v3;  
1120 deuteron order parameter  $S_{CD}$  of bilayers for parameter  
1121 sets Chiu/S4A8, RM/S4A8\_v2, and RM/S4A8\_v3;  
1122 hydration profiles for DLPC, DMPC, DOPC, and  
1123 POPC bilayers across parameter sets; phosphocholine  
1124 moieties SASA; head group orientation, lipid tail  
1125 comparison and parameter set comparison; diffusion  
1126 coefficient of DPPC in control simulations; snapshot of  
1127 DPPC patch partially in gel phase; key properties of  
1128 POPE bilayer for parameter sets Chiu/S4A8/CH0 and  
1129 RM/S4A8/CH0; key properties of POPG bilayer for  
1130 parameter set RM/S4A8/CH0; scheme of the 1LFC  
1131 orientations; 1LFC orientation with respect to mem-  
1132 brane plane along simulations (SI Figures 1–30) (PDF)

1133 Simulation of LFC on a bacterial membrane for both  
1134 parameter sets Chiu/S4A8 (left half) and RM/S4A8\_v1  
1135 (right half), starting from orientation OII (Movie 1)  
1136 (MP4)

## 1139 ■ AUTHOR INFORMATION

## 1140 Corresponding Author

1141 \*E-mail: franca.fraternali@kcl.ac.uk.

## 1142 ORCID

1143 Irene Marzuoli: 0000-0001-7536-6144

1144 Franca Fraternali: 0000-0002-3143-6574

## 1145 Notes

1146 The authors declare no competing financial interest.  
 1147 The topology and the parameter files in GROMACS format for  
 1148 the lipid molecules and the atomic coordinates of equilibrated  
 1149 bilayers of DLPC, DMPC, DOPC, POPC, DPPC, POPE, and  
 1150 POPG are available at <http://fraternalilab.kcl.ac.uk/>  
 1151 [wordpress/biomembrane-simulations](#). Note that these param-  
 1152 eter files include the post-translationally modified residues  
 1153 specified for the GROMOS 54A8 force field earlier.<sup>122</sup>

## 1154 ■ ACKNOWLEDGMENTS

1155 The authors thank Chris Oostenbrink and Maria M. Reif for  
 1156 careful reading of the manuscript and feedback. I.M.  
 1157 acknowledges funding by the Engineering and Physical  
 1158 Sciences Research Council (EPSRC) through the Centre for  
 1159 Doctoral Training “Cross Disciplinary Approaches to Non-  
 1160 Equilibrium Systems” (CANES, Grant No. EP/L015854/1).  
 1161 C.M. acknowledges funding by the MRC/BBSRC Systems  
 1162 Immunology of the Lifecourse programme grant: MABRA  
 1163 “Multiscale analysis of B cell responses in ageing” (MR/  
 1164 L01257X/1). This work was performed using resources  
 1165 provided by the Cambridge Service for Data Driven Discovery  
 1166 (CSD3) operated by the University of Cambridge Research  
 1167 Computing Service (<http://www.cs3.cam.ac.uk/>), provided  
 1168 by Dell EMC and Intel using Tier-2 funding from the  
 1169 Engineering and Physical Sciences Research Council (capital  
 1170 grant EP/P020259/1), and DiRAC funding from the Science  
 1171 and Technology Facilities Council ([www.dirac.ac.uk](http://www.dirac.ac.uk)).

## 1172 ■ REFERENCES

- 1173 (1) Cooper, G. M. *Transport of Small Molecules*; Sinauer Associates, 2000.
- 1174 (2) Cocucci, E.; Kim, J.; Bai, Y.; Pabla, N. Role of Passive Diffusion, Transporters, and Membrane Trafficking-Mediated Processes in Cellular Drug Transport. *Clin. Pharmacol. Ther.* **2017**, *101*, 121–129.
- 1175 (3) Mällkiä, A.; Murtomäki, L.; Urtti, A.; Kontturi, K. Drug permeation in biomembranes: In vitro and in silico prediction and influence of physicochemical properties. *Eur. J. Pharm. Sci.* **2004**, *23*, 13–47.
- 1176 (4) Scott, D.; Ghosh, A.; Di, L.; Maurer, T. Passive drug permeation through membranes and cellular distribution. *Pharmacol. Res.* **2017**, *117*, 94–102.
- 1177 (5) Zhao, R.; Babani, S.; Gao, F.; Liu, L.; Goldman, I. D. The mechanism of transport of the multitargeted antifolate (MTA) and its cross-resistance pattern in cells with markedly impaired transport of methotrexate. *Clin. Cancer Res.* **2000**, *6*, 3687–3695.
- 1178 (6) Shi, Y.; Massagué, J. Mechanisms of TGF-β Signaling from Cell Membrane to the Nucleus. *Cell* **2003**, *113*, 685–700.
- 1179 (7) Jean-Louis, S.; Akare, S.; Ali, M. A.; Mash, E. A.; Meuillet, E.; Martinez, J. D. Deoxycholic acid induces intracellular signaling through membrane perturbations. *J. Biol. Chem.* **2006**, *281*, 14948–14960.
- 1180 (8) Hodder, A. N.; Crewther, P. E.; Anders, R. F. Specificity of the protective antibody response to apical membrane antigen 1. *Infect. Immun.* **2001**, *69*, 3286–3294.
- 1181 (9) Fahy, E.; Subramaniam, S.; Brown, H. A.; Glass, C. K.; Merrill, A. H.; Murphy, R. C.; Raetz, C. R. H.; Russell, D. W.; Seyama, Y.; Shaw, W.; Shimizu, T.; Spener, F.; van Meer, G.; VanNieuwenhze, M.

- S.; White, S. H.; Witztum, J. L.; Dennis, E. A. A comprehensive classification system for lipids. *J. Lipid Res.* **2005**, *46*, 839–862.
- (10) Sharpe, H. J.; Stevens, T. J.; Munro, S. A comprehensive comparison of transmembrane domains reveals organelle-specific properties. *Cell* **2010**, *142*, 158–169.
- (11) Entova, S.; Billod, J.-M.; Swiecicki, J.-M.; Martín-Santamaría, S.; Imperiali, B. Insights into the key determinants of membrane protein topology enable the identification of new monotopic folds. *eLife* **2018**, *7*, No. e40889.
- (12) Zhang, L.; Rozek, A.; Hancock, R. E. Interaction of cationic antimicrobial peptides with model membranes. *J. Biol. Chem.* **2001**, *276*, 35714–35722.
- (13) Risselada, H. J.; Marrink, S. J. The molecular face of lipid rafts in model membranes. *Proc. Natl. Acad. Sci. U.S.A.* **2008**, *105*, 17367–17372.
- (14) Chan, Y.-H. M.; Boxer, S. G. Model membrane systems and their applications. *Curr. Opin. Chem. Biol.* **2007**, *11*, 581–587.
- (15) Nagle, J. F.; Tristram-Nagle, S. Structure of lipid bilayers. *Biochim. Biophys. Acta* **2000**, *1469*, 159–195.
- (16) Kučerka, N.; Heberle, F.; Pan, J.; Katsaras, J. Structural Significance of Lipid Diversity as Studied by Small Angle Neutron and X-ray Scattering. *Membranes* **2015**, *5*, 454–472.
- (17) Pan, J.; Heberle, F. A.; Tristram-Nagle, S.; Szymanski, M.; Koepfinger, M.; Katsaras, J.; Kučerka, N. Molecular structures of fluid phase phosphatidylglycerol bilayers as determined by small angle neutron and X-ray scattering. *Biochim. Biophys. Acta, Biomembr.* **2012**, *1818*, 2135–2148.
- (18) Kučerka, N.; Nieh, M.-P.; Katsaras, J. Fluid phase lipid areas and bilayer thicknesses of commonly used phosphatidylcholines as a function of temperature. *Biochim. Biophys. Acta, Biomembr.* **2011**, *1808*, 2761–2771.
- (19) Gurtovenko, A. A.; Vattulainen, I. Molecular Mechanism for Lipid Flip-Flops. *J. Phys. Chem. B* **2007**, *111*, 13554–13559.
- (20) Tielemans, D.; Marrink, S.-J. Lipids Out of Equilibrium: Energetics of Desorption and Pore Mediated Flip-Flop. *J. Am. Chem. Soc.* **2006**, *128*, 12462–12467.
- (21) Marrink, S.-J.; Mark, A. E. The Mechanism of Vesicle Fusion as Revealed by Molecular Dynamics Simulations. *J. Am. Chem. Soc.* **2003**, *11144*.
- (22) de Vries, A. H.; Mark, A. E.; Marrink, S.-J. Molecular Dynamics Simulation of the Spontaneous Formation of a Small DPPC Vesicle in Water in Atomistic Detail. *J. Am. Chem. Soc.* **2004**, *126*, 4488–4489.
- (23) Marrink, S.-J.; Risselada, J.; Mark, A. E. Simulation of gel phase formation and melting in lipid bilayers using a coarse grained model. *Chem. Phys. Lipids* **2005**, *135*, 223–244.
- (24) Marrink, S.-J.; Lindahl, E.; Edholm, O.; Mark, A. E. Simulation of the Spontaneous Aggregation of Phospholipids into Bilayers. *J. Am. Chem. Soc.* **2001**, *123*, 8638–8639.
- (25) Skjekvål, Å. A.; Madej, B. D.; Dickson, C. J.; Teigen, K.; Walker, R. C.; Gould, I. R. All-atom lipid bilayer self-assembly with the AMBER and CHARMM lipid force fields. *Chem. Commun.* **2015**, *51*, 4402–4405.
- (26) Vernier, P. T.; Ziegler, M. J.; Sun, Y.; Chang, W. V.; Gundersen, M. A.; Tielemans, D. P. Nanopore Formation and Phosphatidylserine Externalization in a Phospholipid Bilayer at High Transmembrane Potential. *J. Am. Chem. Soc.* **2006**, *128*, 6288–6289.
- (27) Leontiadou, H.; Mark, A. E.; Marrink, S.-J. Ion transport across transmembrane pores. *Biophys. J.* **2007**, *92*, 4209–4215.
- (28) Marrink, S.-J.; Jähnig, F.; Berendsen, H. J. Proton transport across transient single-file water pores in a lipid membrane studied by molecular dynamics simulations. *Biophys. J.* **1996**, *71*, 632–647.
- (29) Leontiadou, H.; Mark, A. E.; Marrink, S.-J. Molecular dynamics simulations of hydrophilic pores in lipid bilayers. *Biophys. J.* **2004**, *86*, 2156–2164.
- (30) Sengupta, D.; Leontiadou, H.; Mark, A. E.; Marrink, S.-J. Toroidal pores formed by antimicrobial peptides show significant disorder. *Biochim. Biophys. Acta, Biomembr.* **2008**, *1778*, 2308–2317.
- (31) Leontiadou, H.; Mark, A. E.; Marrink, S.-J. Antimicrobial Peptides in Action. *J. Am. Chem. Soc.* **2006**, *128*, 12156–12161.

- 1270 (32) Lipkin, R.; Pino-Angeles, A.; Lazaridis, T. Transmembrane  
1271 Pore Structures of  $\beta$ -Hairpin Antimicrobial Peptides by All-Atom  
1272 Simulations. *J. Phys. Chem. B* **2017**, *121*, 9126–9140.
- 1273 (33) Piggot, T. J.; Holdbrook, D. A.; Khalid, S. Electroporation of  
1274 the *E. coli* and *S. aureus* Membranes: Molecular Dynamics Simulations  
1275 of Complex Bacterial Membranes. *J. Phys. Chem. B* **2011**, *115*,  
1276 13381–13388.
- 1277 (34) Khalid, S.; Berglund, N. A.; Holdbrook, D. A.; Leung, Y. M.;  
1278 Parkin, J. The membranes of Gram-negative bacteria: progress in  
1279 molecular modelling and simulation. *Biochem. Soc. Trans.* **2015**, *43*,  
1280 162–167.
- 1281 (35) Pino-Angeles, A.; Leveritt, J. M.; Lazaridis, T. Pore Structure  
1282 and Synergy in Antimicrobial Peptides of the Magainin Family. *PLOS*  
1283 *Comput. Biol.* **2016**, *12*, No. e1004570.
- 1284 (36) Lopes, D.; Jakobtorweihen, S.; Nunes, C.; Sarmento, B.; Reis, S.  
1285 Shedding light on the puzzle of drug-membrane interactions:  
1286 Experimental techniques and molecular dynamics simulations. *Prog.*  
1287 *Lipid Res.* **2017**, *65*, 24–44.
- 1288 (37) Klauda, J. B.; Venable, R. M.; Freites, J. A.; O'Connor, J. W.;  
1289 Tobias, D. J.; Mondragon-Ramirez, C.; Vorobyov, I.; MacKerell, A.  
1290 D.; Pastor, R. W. Update of the CHARMM All-Atom Additive Force  
1291 Field for Lipids: Validation on Six Lipid Types. *J. Phys. Chem. B* **2010**,  
1292 *114*, 7830–7843.
- 1293 (38) Hart, K.; Foloppe, N.; Baker, C. M.; Denning, E. J.; Nilsson, L.;  
1294 MacKerell, A. D. Optimization of the CHARMM Additive Force  
1295 Field for DNA: Improved Treatment of the BI/BII Conformational  
1296 Equilibrium. *J. Chem. Theory Comput.* **2012**, *8*, 348–362.
- 1297 (39) Huang, J.; Rauscher, S.; Nawrocki, G.; Ran, T.; Feig, M.; de  
1298 Groot, B. L.; Grubmüller, H.; MacKerell, A. D. CHARMM36m: an  
1299 improved force field for folded and intrinsically disordered proteins.  
1300 *Nat. Methods* **2017**, *14*, 71–73.
- 1301 (40) Maier, J. A.; Martinez, C.; Kasavajhala, K.; Wickstrom, L.;  
1302 Hauser, K. E.; Simmerling, C. ff14SB: Improving the Accuracy of  
1303 Protein Side Chain and Backbone Parameters from ff99SB. *J. Chem.*  
1304 *Theory Comput.* **2015**, *11*, 3696–3713.
- 1305 (41) Scott, W.; Hünenberger, P.; Tironi, I.; Mark, A.; Billeter, S.;  
1306 Fennen, J.; Torda, A.; Huber, T.; Krüger, P.; van Gunsteren, W. F.  
1307 The GROMOS Biomolecular Simulation Program Package. *J. Phys.*  
1308 *Chem. A* **1999**, *103*, 3596–3607.
- 1309 (42) Chiu, S.-W.; Clark, M.; Balaji, V.; Subramaniam, S.; Scott, H.  
1310 L.; Jakobsson, E. Incorporation of surface tension into molecular  
1311 dynamics simulation of an interface: a fluid phase lipid bilayer  
1312 membrane. *Biophys. J.* **1995**, *69*, 1230–1245.
- 1313 (43) Tieleman, D. P.; Berendsen, H. J. C. Molecular dynamics  
1314 simulations of a fully hydrated dipalmitoylphosphatidylcholine bilayer  
1315 with different macroscopic boundary conditions and parameters. *J.*  
1316 *Chem. Phys.* **1996**, *105*, 4871.
- 1317 (44) Poger, D.; Van Gunsteren, W. F.; Mark, A. E. A new force field  
1318 for simulating phosphatidylcholine bilayers. *J. Comput. Chem.* **2010**,  
1319 *31*, 1117–1125.
- 1320 (45) Chandrasekhar, I.; Kastenholz, M.; Lins, R. D.; Oostenbrink,  
1321 C.; Schuler, L. D.; Tieleman, D. P.; van Gunsteren, W. F. A consistent  
1322 potential energy parameter set for lipids: dipalmitoylphosphatidylcho-  
1323 line as a benchmark of the GROMOS96 45A3 force field. *Eur.*  
1324 *Biophys. J.* **2003**, *32*, 67–77.
- 1325 (46) Kukol, A. Lipid Models for United-Atom Molecular Dynamics  
1326 Simulations of Proteins. *J. Chem. Theory Comput.* **2009**, *5*, 615–626.
- 1327 (47) Reif, M. M.; Hünenberger, P. H.; Oostenbrink, C. New  
1328 Interaction Parameters for Charged Amino Acid Side Chains in the  
1329 GROMOS Force Field. *J. Chem. Theory Comput.* **2012**, *8*, 3705–3723.
- 1330 (48) Margreitter, C.; Reif, M. M.; Oostenbrink, C. Update on  
1331 phosphate and charged post-translationally modified amino acid  
1332 parameters in the GROMOS force field. *J. Comput. Chem.* **2017**, *38*,  
1333 714–720.
- 1334 (49) Chandrasekhar, I.; van Gunsteren, W. F. Sensitivity of  
1335 molecular dynamics simulations of lipids to the size of the ester  
1336 carbon. *Curr. Sci.* **2001**, 1325–1327.
- 1337 (50) Chandrasekhar, I.; van Gunsteren, W. F. A comparison of the  
1338 potential energy parameters of aliphatic alkanes: molecular dynamics  
simulations of triacylglycerols in the alpha phase. *Eur. Biophys. J.* **2002**, *31*, 89–101.
- (51) Schmid, N.; Eichenberger, A. P.; Choutko, A.; Riniker, S.; Winger, M.; Mark, A. E.; van Gunsteren, W. F. Definition and testing of the GROMOS force-field versions 54A7 and 54B7. *Eur. Biophys. J.* **2011**, *40*, 843–856.
- (52) Bransden, B. H.; Joachain, C. *J. Physics of Atoms and Molecules*; Prentice Hall, 2003; p 1114.
- (53) Mulliken, R. S. Electronic Population Analysis on LCAO-MO Molecular Wave Functions. *I. J. Chem. Phys.* **1955**, *23*, 1833–1840.
- (54) Reif, M. M.; Winger, M.; Oostenbrink, C. Testing of the GROMOS Force-Field Parameter Set 54A8: Structural Properties of Electrolyte Solutions, Lipid Bilayers, and Proteins. *J. Chem. Theory Comput.* **2013**, *9*, 1247–1264.
- (55) Berglund, N. A.; Piggot, T. J.; Jefferies, D.; Sessions, R. B.; Bond, P. J.; Khalid, S. Interaction of the Antimicrobial Peptide Polymyxin B1 with Both Membranes of *E. coli*: A Molecular Dynamics Study. *PLOS Comput. Biol.* **2015**, *11*, No. e1004180.
- (56) Chandrasekhar, I.; Oostenbrink, C.; van Gunsteren, W. F. Simulating the Physiological Phase of Hydrated DPPC Bilayers: The Ester Moiety. *Soft Mater.* **2004**, *2*, 27–45.
- (57) Oostenbrink, C.; Villa, A.; Mark, A. E.; Van Gunsteren, W. F. A biomolecular force field based on the free enthalpy of hydration and solvation: The GROMOS force-field parameter sets 53A5 and 53A6. *J. Comput. Chem.* **2004**, *25*, 1656–1676.
- (58) Poger, D.; Mark, A. E. On the Validation of Molecular Dynamics Simulations of Saturated and cis -Monounsaturated Phosphatidylcholine Lipid Bilayers: A Comparison with Experiment. *J. Chem. Theory Comput.* **2010**, *6*, 325–336.
- (59) Tironi, I. G.; Sperb, R.; Smith, P. E.; van Gunsteren, W. F. A generalized reaction field method for molecular dynamics simulations. *J. Chem. Phys.* **1995**, *102*, 5451–5459.
- (60) Abraham, M. J.; van der Spoel, D.; Lindahl, E.; Hess, B. *GROMACS User Manual*, version 2016; GROMACS Development Team, 2018.
- (61) Essmann, U.; Perera, L.; Berkowitz, M. L.; Darden, T.; Lee, H.; Pedersen, L. G. A smooth particle mesh Ewald method. *J. Chem. Phys.* **1995**, *103*, 8577–8593.
- (62) Pluhackova, K.; Kirsch, S. A.; Han, J.; Sun, L.; Jiang, Z.; Unruh, T.; Böckmann, R. A. A Critical Comparison of Biomembrane Force Fields: Structure and Dynamics of Model DMPC, POPC, and POPE Bilayers. *J. Phys. Chem. B* **2016**, *120*, 3888–3903.
- (63) Lewis, R. N. A. H.; Mak, N.; McElhaney, R. N. A differential scanning calorimetric study of the thermotropic phase behavior of model membranes composed of phosphatidylcholines containing linear saturated fatty acyl chains. *Biochemistry* **1987**, *26*, 6118–6126.
- (64) Huang, C. H.; Lapides, J. R.; Levin, I. W. Phase-transition behavior of saturated, symmetric chain phospholipid bilayer dispersions determined by Raman spectroscopy: correlation between spectral and thermodynamic parameters. *J. Am. Chem. Soc.* **1982**, *104*, 5926–5930.
- (65) Mabrey, S.; Sturtevant, J. M. Investigation of phase transitions of lipids and lipid mixtures by sensitivity differential scanning calorimetry. *Proc. Natl. Acad. Sci. U.S.A.* **1976**, *73*, 3862–3866.
- (66) Davis, P. J.; Fleming, B. D.; Coolbear, K. P.; Keough, K. M. W. Gel to liquid-crystalline transition temperatures of water dispersions of two pairs of positional isomers of unsaturated mixed-acid phosphatidylcholines. *Biochemistry* **1981**, *20*, 3633–3636.
- (67) Wang, Z. Q.; Lin, H. N.; Li, S.; Huang, C. H. Calorimetric studies and molecular mechanics simulations of monounsaturated phosphatidylethanolamine bilayers. *J. Biol. Chem.* **1994**, *269*, 23491–23499.
- (68) Borle, F.; Seelig, J.  $\text{Ca}^{2+}$  binding to phosphatidylglycerol bilayers as studied by differential scanning calorimetry and  $^2\text{H}$ - and  $^{31}\text{P}$ -nuclear magnetic resonance. *Chem. Phys. Lipids* **1985**, *36*, 263–283.
- (69) Berendsen, H. J.; van der Spoel, D.; van Drunen, R. GROMACS: A message-passing parallel molecular dynamics implementation. *Comput. Phys. Commun.* **1995**, *91*, 43–56.

- 1408 (70) Abraham, M. J.; Murtola, T.; Schulz, R.; Páll, S.; Smith, J. C.;  
1409 Hess, B.; Lindahl, E. GROMACS: High performance molecular  
1410 simulations through multi-level parallelism from laptops to super-  
1411 computers. *SoftwareX* **2015**, *1–2*, 19–25.
- 1412 (71) Berendsen, H. J. C.; Postma, J. P. M.; van Gunsteren, W. F.;  
1413 DiNola, A.; Haak, J. R. Molecular dynamics with coupling to an  
1414 external bath. *J. Chem. Phys.* **1984**, *81*, 3684–3690.
- 1415 (72) Hess, B.; Bekker, H.; Berendsen, H. J. C.; Fraaije, J. G. E. M.  
1416 LINCS: A linear constraint solver for molecular simulations. *J.  
1417 Comput. Chem.* **1997**, *18*, 1463–1472.
- 1418 (73) Miyamoto, S.; Kollman, P. A. Settle: An analytical version of  
1419 the SHAKE and RATTLE algorithm for rigid water models. *J.  
1420 Comput. Chem.* **1992**, *13*, 952–962.
- 1421 (74) Poger, D.; Caron, B.; Mark, A. E. Validating lipid force fields  
1422 against experimental data: Progress, challenges and perspectives.  
1423 *Biochim. Biophys. Acta, Biomembr.* **2016**, *1858*, 1556–1565.
- 1424 (75) Braun, A. R.; Brandt, E. G.; Edholm, O.; Nagle, J. F.; Sachs, J.  
1425 N. Determination of electron density profiles and area from  
1426 simulations of undulating membranes. *Biophys. J.* **2011**, *100*, 2112–  
1427 2120.
- 1428 (76) Chiu, S.-W.; Pandit, S. A.; Scott, H. L.; Jakobsson, E. An  
1429 Improved United Atom Force Field for Simulation of Mixed Lipid  
1430 Bilayers. *J. Phys. Chem. B* **2009**, *113*, 2748–2763.
- 1431 (77) Ding, W.; Palaiokostas, M.; Wang, W.; Orsi, M. Effects of Lipid  
1432 Composition on Bilayer Membranes Quantified by All-Atom  
1433 Molecular Dynamics. *J. Phys. Chem. B* **2015**, *119*, 15263–15274.
- 1434 (78) Gurtovenko, A. A.; Vattulainen, I. Calculation of the  
1435 electrostatic potential of lipid bilayers from molecular dynamics  
1436 simulations: Methodological issues. *J. Chem. Phys.* **2009**, *130*,  
1437 No. 215107.
- 1438 (79) Einstein, A.; Fürt, R. *Investigations on the Theory of Brownian  
1439 Movement*; Dover Publications, 1956; p 119.
- 1440 (80) Johner, N.; Harries, D.; Khelashvili, G. Implementation of a  
1441 methodology for determining elastic properties of lipid assemblies  
1442 from molecular dynamics simulations. *BMC Bioinf.* **2016**, *17*, No. 161.
- 1443 (81) Biasini, M.; Mariani, V.; Haas, J.; Scheuber, S.; Schenk, A. D.;  
1444 Schwede, T.; Philippse, A. OpenStructure: a flexible software  
1445 framework for computational structural biology. *Bioinformatics* **2010**,  
1446 *26*, 2626–2628.
- 1447 (82) Aurenhammer, F. Franz, Voronoi diagrams – a survey of a  
1448 fundamental geometric data structure. *ACM Comput. Surv.* **1991**, *23*,  
1449 345–405.
- 1450 (83) Uppulury, K.; Coppock, P. S.; Kindt, J. T. Molecular Simulation  
1451 of the DPPE Lipid Bilayer Gel Phase: Coupling between Molecular  
1452 Packing Order and Tail Tilt Angle. *J. Phys. Chem. B* **2015**, *119*, 8725.
- 1453 (84) Reißer, S.; Poger, D.; Stroet, M.; Mark, A. E. Real Cost of  
1454 Speed: The Effect of a Time-Saving Multiple-Time-Stepping  
1455 Algorithm on the Accuracy of Molecular Dynamics Simulations. *J.  
1456 Chem. Theory Comput.* **2017**, *13*, 2367–2372.
- 1457 (85) Arézo, C.; de Vries, A. H.; Höltje, H.-D.; Tielemans, D. P.;  
1458 Marrink, S.-J. Methodological Issues in Lipid Bilayer Simulations. *J.  
1459 Phys. Chem. B* **2003**, *107*, 9424–9433.
- 1460 (86) Chowdhary, J.; Harder, E.; Lopes, P. E. M.; Huang, L.;  
1461 MacKerell, A. D.; Roux, B. A Polarizable Force Field of  
1462 Dipalmitoylphosphatidylcholine Based on the Classical Drude  
1463 Model for Molecular Dynamics Simulations of Lipids. *J. Phys.  
1464 Chem. B* **2013**, *117*, 9142–9160.
- 1465 (87) Warshavskiak, D. T.; Muellner, M. J.; Chachisvilis, M. Effect of  
1466 membrane tension on the electric field and dipole potential of lipid  
1467 bilayer membrane. *Biochim. Biophys. Acta, Biomembr.* **2011**, *1808*,  
1468 2608–2617.
- 1469 (88) Vermeer, L. S.; de Groot, B. L.; Réat, V.; Milon, A.; Czaplicki, J.  
1470 Acyl chain order parameter profiles in phospholipid bilayers:  
1471 computation from molecular dynamics simulations and comparison  
1472 with  $^2\text{H}$  NMR experiments. *Eur. Biophys. J.* **2007**, *36*, 919–931.
- 1473 (89) Douliez, J. P.; Léonard, A.; Dufourc, E. J. Restatement of order  
1474 parameters in biomembranes: calculation of C-C bond order  
1475 parameters from C-D quadrupolar splittings. *Biophys. J.* **1995**, *68*,  
1476 1727–1739.
- 1477 (90) Petrache, H. I.; Dodd, S. W.; Brown, M. F. Area per lipid and  
1478 acyl length distributions in fluid phosphatidylcholines determined by  
1479  $(2)\text{H}$  NMR spectroscopy. *Biophys. J.* **2000**, *79*, 3172–3192.
- 1480 (91) Borle, F.; Seelig, J. Hydration of Escherichia coli lipids:  
1481 Deuterium T1 relaxation time studies of phosphatidylglycerol,  
1482 phosphatidylethanolamine and phosphatidylcholine. *Biochim. Biophys.  
1483 Acta, Biomembr.* **1983**, *735*, 131–136.
- 1484 (92) Ulrich, A. S.; Volke, F.; Watts, A. The dependence of  
1485 phospholipid head-group mobility on hydration as studied by  
1486 deuterium-NMR spin-lattice relaxation time measurements. *Chem.  
1487 Phys. Lipids* **1990**, *55*, 61–66.
- 1488 (93) Ulrich, A.; Watts, A. Molecular response of the lipid headgroup  
1489 to bilayer hydration monitored by  $^2\text{H}$ -NMR. *Biophys. J.* **1994**, *66*,  
1490 1441–1449.
- 1491 (94) Lairion, F.; Filler, R.; Disalvo, E. Reversed micelles as model  
1492 systems to study interfacial properties of lipid bilayers. *Colloids Surf., B  
1493 2002*, *25*, 369–371.
- 1494 (95) Semchyschyn, D. J.; Macdonald, P. M. Conformational  
1495 response of the phosphatidylcholine headgroup to bilayer surface  
1496 charge: torsion angle constraints from dipolar and quadrupolar  
1497 couplings in bicelles. *Magn. Reson. Chem.* **2004**, *42*, 89–104.
- 1498 (96) Doux, J. P. F.; Hall, B. A.; Killian, J. A. How lipid headgroups  
1499 sense the membrane environment: an application of  $^{14}\text{N}$  NMR.  
1500 *Biophys. J.* **2012**, *103*, 1245–1253.
- 1501 (97) Büldt, G.; Gally, H. U.; Seelig, A.; Seelig, J.; Zaccai, G. Neutron  
1502 diffraction studies on selectively deuterated phospholipid bilayers.  
1503 *Nature* **1978**, *271*, 182–184.
- 1504 (98) Botan, A.; Favela-Rosales, F.; Fuchs, P. F. J.; Javanainen, M.;  
1505 Kanduč, M.; Kulig, W.; Lamberg, A.; Loison, C.; Lyubartsev, A.;  
1506 Miettinen, M. S.; Monticelli, L.; Määttä, J.; Ollila, O. H. S.; Retegan,  
1507 M.; Rög, T.; Santuz, H.; Tynkkynen, J. Toward Atomistic Resolution  
1508 Structure of Phosphatidylcholine Headgroup and Glycerol Backbone  
1509 at Different Ambient Conditions. *J. Phys. Chem. B* **2015**, *119*, 15075–  
1510 15088.
- 1511 (99) Venable, R. M.; Ingólfsson, H. I.; Lerner, M. G.; Perrin, B. S.;  
1512 Camley, B. A.; Marrink, S. J.; Brown, F. L. H.; Pastor, R. W. Lipid and  
1513 Peptide Diffusion in Bilayers: The Saffman-Delbrück Model and  
1514 Periodic Boundary Conditions. *J. Phys. Chem. B* **2017**, *121*, 3443–  
1515 3457.
- 1516 (100) Vögele, M.; Köfinger, J.; Hummer, G. Hydrodynamics of  
1517 Diffusion in Lipid Membrane Simulations. *Phys. Rev. Lett.* **2018**, *120*,  
1518 No. 268104.
- 1519 (101) Lindblom, G.; Orädd, G. Lipid lateral diffusion and membrane  
1520 heterogeneity. *Biochim. Biophys. Acta, Biomembr.* **2009**, *1788*, 234–  
1521 244.
- 1522 (102) Poger, D.; Mark, A. E. Lipid Bilayers: The Effect of Force  
1523 Field on Ordering and Dynamics. *J. Chem. Theory Comput.* **2012**, *8*,  
1524 4807–4817.
- 1525 (103) Piggot, T. J.; Piñeiro, Á.; Khalid, S. Molecular Dynamics  
1526 Simulations of Phosphatidylcholine Membranes: A Comparative  
1527 Force Field Study. *J. Chem. Theory Comput.* **2012**, *8*, 4593–4609.
- 1528 (104) Nagle, J. F. Experimentally determined tilt and bending  
1529 moduli of single-component lipid bilayers. *Chem. Phys. Lipids* **2017**,  
1530 205, 18–24.
- 1531 (105) Doktorova, M.; Harries, D.; Khelashvili, G. Determination of  
1532 bending rigidity and tilt modulus of lipid membranes from real-space  
1533 fluctuation analysis of molecular dynamics simulations. *Phys. Chem.  
1534 Chem. Phys.* **2017**, *19*, 16806–16818.
- 1535 (106) Nagle, J. F.; Cognet, P.; Dupuy, F. G.; Tristram-Nagle, S.  
1536 Structure of gel phase DPPC determined by X-ray diffraction. *Chem.  
1537 Phys. Lipids* **2019**, *218*, 168–177.
- 1538 (107) Sun, W.-J.; Suter, R. M.; Knewton, M. A.; Worthington, C.  
1539 R.; Tristram-Nagle, S.; Zhang, R.; Nagle, J. F. Order and disorder in  
1540 fully hydrated unoriented bilayers of gel-phase dipalmitoylphospho-  
1541 tidylcholine. *Phys. Rev. E* **1994**, *49*, 4665–4676.
- 1542 (108) McIntosh, T. J.; Simon, S. A. Area per molecule and  
1543 distribution of water in fully hydrated dilrauroylphosphatidylethanol-  
1544 amine bilayers. *Biochemistry* **1986**, *25*, 4948–4952.

- 1545 (109) Marinov, R.; Dufourc, E. J. Thermotropism and hydration  
1546 properties of POPE and POPE-cholesterol systems as revealed by  
1547 solid state<sup>2</sup>H and <sup>31</sup>P-NMR. *Eur. Biophys. J.* **1996**, *24*, 423–431.  
1548 (110) Rand, R. P.; Fuller, N.; Parsegian, V. A.; Rau, D. C. Variation  
1549 in hydration forces between neutral phospholipid bilayers: evidence  
1550 for hydration attraction. *Biochemistry* **1988**, *27*, 7711–7722.  
1551 (111) Hwang, P. M.; Zhou, N.; Shan, X.; Arrowsmith, C. H.; Vogel,  
1552 H. J. Three-Dimensional Solution Structure of Lactoferricin B, an  
1553 Antimicrobial Peptide Derived from Bovine Lactoferrin <sup>†</sup>. *Biochemistry*  
1554 **1998**, *37*, 4288–4298.  
1555 (112) Nguyen, L. T.; Schibli, D. J.; Vogel, H. J. Structural studies  
1556 and model membrane interactions of two peptides derived from  
1557 bovine lactoferricin. *J. Pept. Sci. A* **2005**, *11*, 379–389.  
1558 (113) Schibli, D. J.; Hwang, P. M.; Vogel, H. J. The structure of the  
1559 antimicrobial active center of lactoferricin B bound to sodium dodecyl  
1560 sulfate micelles. *FEBS Lett.* **1999**, *446*, 213–217.  
1561 (114) Sohlenkamp, C.; Geiger, O. Bacterial membrane lipids:  
1562 diversity in structures and pathways. *FEMS Microbiol. Rev.* **2016**, *40*,  
1563 133–159.  
1564 (115) Ma, H.; Cummins, D. D.; Edelstein, N. B.; Gomez, J.; Khan,  
1565 A.; Llewellyn, M. D.; Picudella, T.; Willsey, S. R.; Nangia, S. Modeling  
1566 Diversity in Structures of Bacterial Outer Membrane Lipids. *J. Chem.*  
1567 *Theory Comput.* **2017**, *13*, 811–824.  
1568 (116) Castelletto, V.; de Santis, E.; Alkassem, H.; Lamarre, B.;  
1569 Noble, J. E.; Ray, S.; Bella, A.; Burns, J. R.; Hoogenboom, B. W.;  
1570 Ryadnov, M. G. Structurally plastic peptide capsules for synthetic  
1571 antimicrobial viruses. *Chem. Sci.* **2016**, *7*, 1707–1711.  
1572 (117) Kandasamy, S. K.; Larson, R. G. Binding and insertion of  $\alpha$ -  
1573 helical anti-microbial peptides in POPC bilayers studied by molecular  
1574 dynamics simulations. *Chem. Phys. Lipids* **2004**, *132*, 113–132.  
1575 (118) Vivcharuk, V.; Tomberli, B.; Tolokh, I. S.; Gray, C. G.  
1576 Prediction of binding free energy for adsorption of antimicrobial  
1577 peptide lactoferricin B on a POPC membrane. *Phys. Rev. E* **2008**, *77*,  
1578 No. 031913.  
1579 (119) Wang, Y.; Schlamadinger, D. E.; Kim, J. E.; McCammon, J. A.  
1580 Comparative molecular dynamics simulations of the antimicrobial  
1581 peptide CM15 in model lipid bilayers. *Biochim. Biophys. Acta,*  
1582 *Biomembr.* **2012**, *1818*, 1402–1409.  
1583 (120) Strøm, M. B.; Haug, B. E.; Rekdal, O.; Skar, M. L.; Stensen,  
1584 W.; Svendsen, J. S. Important structural features of 15-residue  
1585 lactoferricin derivatives and methods for improvement of antimicro-  
1586 bial activity. *Biochem. Cell Biol.* **2002**, *80*, 65–74.  
1587 (121) Chan, D. I.; Prenner, E. J.; Vogel, H. J. Tryptophan- and  
1588 arginine-rich antimicrobial peptides: Structures and mechanisms of  
1589 action. *Biochim. Biophys. Acta, Biomembr.* **2006**, *1758*, 1184–1202.  
1590 (122) Petrov, D.; Margreitter, C.; Grandits, M.; Oostenbrink, C.;  
1591 Zagrovic, B. A Systematic Framework for Molecular Dynamics  
1592 Simulations of Protein Post-Translational Modifications. *PLoS*  
1593 *Comput. Biol.* **2013**, *9*, No. e1003154.